INSTITUT DE FRANCE
Académie des sciences

Comptes Rendus

Géoscience

Sciences de la Planète

Guy Vasseur

Geothermal heat advected by the recharge of underground conduit. Case study of the karstic spring of Lez (Hérault, France)

Volume 355, Special Issue S1 (2023), p. 533-557

Online since: 12 December 2022

Part of Special Issue: Geo-hydrological Data & Models

Guest editors: Vazken Andréassian (INRAE, France), Valérie Plagnes (Sorbonne Université, France), Craig Simmons (Flinders University, Australia) and Pierre Ribstein (Sorbonne Université, France)

https://doi.org/10.5802/crgeos.163

The Comptes Rendus. Géoscience — Sciences de la Planète *are a member of the Mersenne Center for open scientific publishing*
www.centre-mersenne.org — e-ISSN : 1778-7025

Comptes Rendus
Géoscience — Sciences de la Planète
2023, Vol. 355, Special Issue S1, p. 533-557
https://doi.org/10.5802/crgeos.163

Research article

Geo-hydrological Data & Models

Geothermal heat advected by the recharge of underground conduit. Case study of the karstic spring of Lez (Hérault, France)

Guy Vasseur [a]

[a] Fondation CERGA: Centre pour l'Enseignement et la Recherche en Geosciences et Applications, Résidence Astérie A2, 740 rue Paul Rimbaud, 34080 Montpellier, France
E-mail: guy.vasseur@upmc.fr

Abstract. The karstic flow system of the Lez spring is capturing a large proportion of the deep geothermal heat flow as observed by temperature measurements both above and below the underground karst network. For interpreting these data, an analytical model of heat/fluid interaction based on the conservation of mass and energy in a dual conduit/porous medium system is developed. In the model of energy transport, the energy of the fluid includes its enthalpy plus its gravity potential; the hydraulic head is shown to be the correct potential accounting for both pressure and gravity. The thermal features of the model are expressed as a function of a few parameters: from comparison with the actual data, the depth of the conduit appears to lie around 400 m and the number *Pe* characterizing the recharge is about 6. When estimated with available thermal data, the amount of geothermal energy captured by the flow system in steady state conditions is significantly lower than the actual energy output of the spring. The possible origin of this offset is discussed: effect of gravity potential, 3D convergence of geothermal heat flux lines, transient effect. Moreover, the mapping of the vertical temperature gradient at low depth indicates the general pattern of the recharge zone energy.

Keywords. Temperature, Analytical solutions, Groundwater recharge, Energy budget, Karst, Steady state, Gravity potential.

Manuscript received 9 March 2022, revised 5 September 2022, accepted 12 September 2022.

1. Introduction

The temperature of groundwater is a potential tracer of circulation that can provide insights into the dynamics of hydro-geological processes. When the pattern of the groundwater flow is diffuse, either through small pores of the rock matrix or through multiple fractures, the concept of representative elementary volume (REV) in porous media offers a conceptual framework for describing the heat and mass flow [de Marsily, 1995, p. 12, p. 42]. In such a REV, the water fluxes are described by an average quantity (the specific discharge or Darcy velocity) and the thermal state of the rock-water system is characterized by a single temperature. In sedimentary basins, heat transfer in porous media explains satisfactorily the temperature field associated with large scale groundwater flow [Toth, 1963, Smith and Chapman, 1983]. Inversely, very deep temperature data, obtained in oil exploration boreholes for instance [Deming et al., 1992, Vasseur and Demongodin, 1995, Reiter, 2001, Pimentel and Hamza, 2012, Tavares et al., 2014], are currently used to constrain the large scale underground flow in deep aquifers or to derive the field of permeability [Saar, 2011]. In area of high geothermal potential, such as the Snake River Plain (USA), temperature profiles in boreholes and temperature gradients are useful to decipher the underground flow pattern and to infer its geothermal potential [McLing

et al., 2016, Lachmar et al., 2017]. Alternatively, they can be used to estimate the area of the recharge [e.g. Ingebritsen et al., 1989].

In contrast with diffuse type water flow, in karstic aquifers, heat (and fluid) transfer cannot be described simply by transfer in porous media because a major component of the porosity is composed of very large pores and open channels. These conduits are focusing the initial slow water flow of the surrounding fractured medium and present very active flow following the laws of hydraulics. In fact, the surrounding rocks which provide the water recharge toward the localized conduit flow [Atkinson, 1977], can generally be modelled as a porous medium; but inside the conduits, the water fluxes are best modelled by a network of pipes embedded in a porous rock matrix. Hybrid models have been used to simulate the transport of heat and reactive solute transport in coupled porous media and conduits [Liedl and Sauter, 1998, Liedl et al., 2003, Birk et al., 2006, Covington et al., 2011] using mathematical and numerical models.

Many observations show that, when observed elsewhere than directly in karst intersections, the vertical gradient of temperature in karstic areas is generally much lower than expected [Mathey, 1974, Luetscher and Jeannin, 2004]. This suggests that a large proportion of the regional geothermal heat flow may be captured by the water flow and eventually warms the out-flowing waters. Quantitative studies of heat flow processes within the saturated zone of karst systems are available [Benderitter et al., 1993, Lismonde, 2010, Badino, 2005]; these studies are mainly based on the temperature of the karstic conduit whereas the quantitative understanding of the physical interaction between the water flow and the heat flow requires to account not only for the temperature within the conduit, but also for the temperature field inside the surrounding rocks.

This study develops an analytic model describing the temperature field in a system based on the conceptual model of fluvio-karst described by White [2002, 2006]. This model is applied to the actual karstic zone of the Lez spring where a series of thermal data are available. The underground system of the Lez spring, located about 15 km North of the city of Montpellier, is a classical example of “karst barré” [or “damed karst”, Bakalowicz, 2005]; it gives birth to the Lez river which ends southward in the Mediterranean sea (28 km length). The watershed area feeding this spring has had relatively low structural deformation: the geometry of the corresponding underground karstic system is not directly known but it is likely to be relatively horizontal as is the general stratification. The Lez karstic network may thus be considered as a convenient example of underground sub-horizontal conduit.

The generic hydrological model used is illustrated on Figure 1 and is inspired from Ewers and Quinlan [1985]: rain infiltrates in the fractured medium, then merges toward a horizontal open conduit thereby contributing to the horizontal flux toward the natural outlet. Several simplifying assumptions are used: an idealized geometry is assumed and composed of a porous/fractured matrix connected to a horizontal conduit flow bounded by two horizontal planes as illustrated farther by Figure 8. The transverse dimensions of the conduit are small enough so that their internal temperature is nearly homogeneous. Following Bovardsson [1969] and Ziagos and Blackwell [1986] for open fractures—but also Vasseur et al. [2002] and Burns et al. [2016] for a thin horizontal aquifer instead of open conduit—the presence of such a horizontal concentrated flow can be accounted for through a specific boundary condition. This boundary condition, based on the energy and mass budget of the fluid system, is imposed on the limits of the porous medium. Only the steady state temperature is considered which implies that the actual recharge is simplified to an average constant rain. Moreover the porous medium is saturated and the fluid inside the conduit is assumed to be well mixed—or even turbulent—so that it is characterized by a single temperature. Using several other assumptions (mainly a very simple geometry of the flow and a negligible horizontal component of thermal conduction), it is possible to obtain simple analytical functions relating available hydrothermal data to a few hydrogeological parameters. This model is then applied to available observations of the Lez spring to obtain a better understanding of the interaction between the geothermal heat flow and the hydrological system.

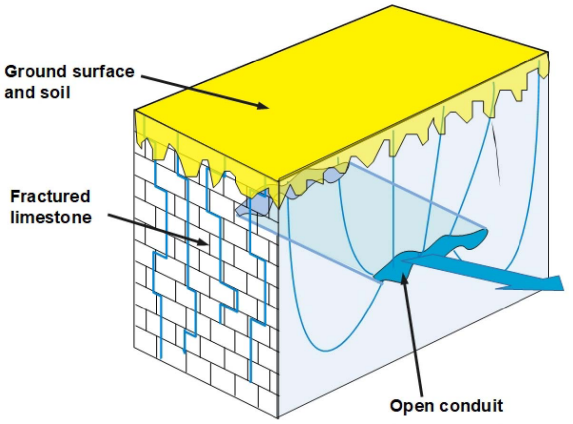

Figure 1. Block-diagram inspired by Ewers and Quinlan [1985] showing the underground flow of water in karstic districts. The two types of water flow are illustrated in blue: slow infiltration in fractured rocks and relatively rapid flow in concentrated conduits.

2. Presentation of the Lez spring system and of its geothermal context

The general context of the Lez spring system has been intensively investigated because it has been for a long time and is still the main source of drinking water for the urban agglomeration of Montpellier [Drogue, 1969, 1985, Lacas, 1976, Avias, 1992, 1995, Guilbot, 1975, Uil, 1978, Bérard, 1983, Botton, 1984, Touet, 1985, Karam, 1989, Malard and Chapuis, 1995, Dausse, 2015].

2.1. *General presentation of the system*

The Lez karstic system belongs to the Mesozoic carbonate series of Languedoc which were deposited from Lias to Cretaceous on the north-western margin of the Tethyan Ocean, controlled by N-E trending faults such as the Cevennes fault (CF on Figure 2) and the Nimes fault (NF on Figure 2) [Husson, 2013]. During Cenozoic times, several geological events have imprinted the area: the Eocene Pyrenean orogeny followed by the Oligocene rifting of the gulf of Lion imposed a drainage system flowing southward and a reactivation of fault systems oriented North-East. The result is a system of large faults (mainly normal to strike slip) in the North to North-East direction as well as thrusts trending in the East–West direction located North of the Montpellier city. The last transgression occurred during early Miocene followed by an uplift during which the base level falls of 1500 m. These episodes have sculpted a large karstic system in such a way as to adapt the drainage hydro-geological flow from mountains North of the Cevennes fault toward the Mediterranean sea to the topographic evolution [Avias, 1992, Bakalowicz, 2005, Husson, 2013].

The watershed of the Lez spring is part of the karstic hydrogeological system called the North Montpellier Garrigue unit, delimited by the Hérault river (to the West) and the Vidourle river (to the North and East). The geological setting and the major tectonic structures characterizing this unit are illustrated in Figure 2 from CERGH [1978]. The karstic aquifer layer has an estimated thickness of 650 to 800 m within the Upper Jurassic layers on both sides of the Matelles Fault (MF on Figure 2) with a thick succession of Lower Valanginian (Lower Cretaceous) marls and marly limestones; the aquifer itself straddles in the Upper Jurassic and the Berriasian (Lower Cretaceous). The karstic conduit has been recognized by diving with a cross sectional width of a few meters at a depth of about 100 m, and was explored only in the vicinity of the spring; the general geometry of the network remains speculative as largely deduced from geological observations and hydrological measurements such as dye, piezometer, chemistry.... [Marechal et al., 2014]. Following a proposition by Dubois [1964] and using hydro-dynamical observations, Karam [1989] speculates on the existence of a single major karstic conduit running from North to South, along the major fault of "les Matelles" ("FM" on Figure 2). The major hydrogeological characteristics of the system have been summarized in Avias [1995]: with a natural overflow lying at 65 m (asl), the Lez spring is the main outlet of a large hydrogeological catchment; its area—illustrated on Figure 2—is estimated around 250 km^2, based on geology, dye tracings, and groundwater level dynamics in the network of observation boreholes during the draw down [Ladouche et al., 2014, Thiery et al., 1983, Dausse, 2015, Marechal et al., 2014]. Its recharge zones include (i) the Jurassic limestone outcrop (between 80 and 100 km^2), (ii) the Cretaceous marly

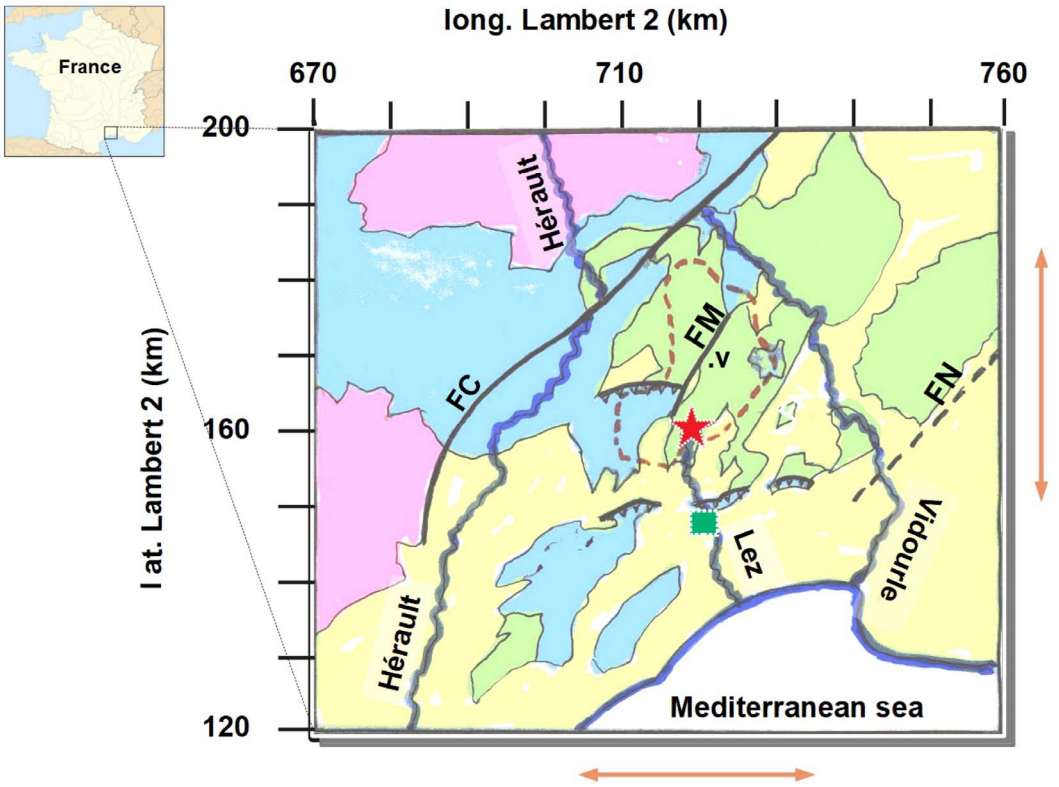

Figure 2. Simplified hydrogeologic map of the Languedoc karstic area with coordinates in km (Lambert 2 projection). The background illustrates the simplified geology: pre-Jurassic (basement to Lias) in pink, Jurassic in blue, Cretaceous in green and Cenozoic (Oligocene to Quaternary) in yellow. The thick lines are the main tectonic accidents: strike slip faults (*FC* for Cevennes fault, *FM* for Matelles fault and *FN* for Nimes fault) and overthrust faults are toothed black lines. The heavy blue lines show the main rivers (Hérault, Lez, Vidourle). The Lez spring is the red star and its recharge basin is shown by a dotted red line. The green square is for the Montpellier town, the symbol "v" for the Valflaunes meteorological station. The horizontal and the vertical orange scale bars present the limits in the EW and NS directions of the studied zone (restricted zone of Figures 3 and 5).

limestone formations through leakage toward the underlying Jurassic. Tertiary formations are generally impervious and contribute insignificantly to the karst aquifer recharge.

For more than 200 years, the Lez spring has been the main supply of drinking water for the city of Montpellier but the equipment for collecting the spring has evolved. Prior to 1968, the resource was exploited through spring overflow collection between 25 and 600 l/s [Paloc, 1979], then from 1968 to 1982, through pumping in the pan hole at a rate of some 800 l/s. Following this period, a so-called "active management" of the Lez karst system was undertaken with pumping rates in the summer periods exceeding the natural discharge; from 1982, deep wells were drilled into the main karst conduit upstream of the spring in order to reach a maximum yield of 2000 l/s [Avias, 1995] through pumping units.

2.2. *Estimate of the average volumetric and energetic discharge*

The natural volumetric discharge of the karst system is not directly observed, because the Lez spring has been tapped since 1854. However, its pumping rate has been measured since 1974 and the spring's residual overflow discharges were reliably measured between 1987 and 2007. From these observations,

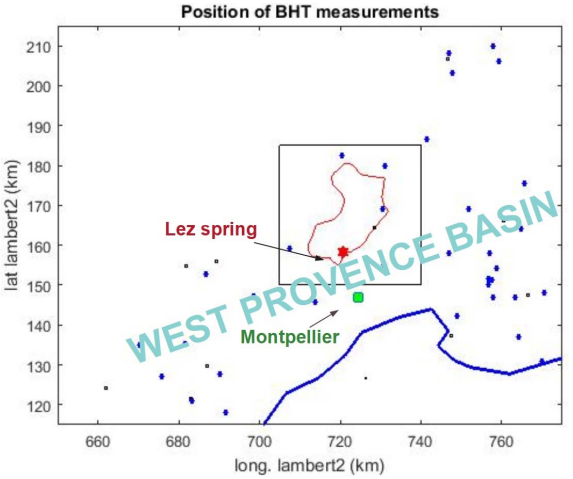

Figure 3. Location of the deep exploration boreholes in the western part of the South Provence basin where BHT temperature measurements are available. The green square is the town of Montpellier, the red star is the Lez spring and the red curve bounds its surface recharge. A restricted 35×30 km^2 area around this recharge area is shown by a rectangular inset and corresponds to the range illustrated by orange arrows of Figure 2.

the yearly flow is about 62×10^6 m^3·y^{-1} which corresponds to a mean of about 2 m^3·s^{-1}. In fact, during floods, the instantaneous flow rate may exceed 10 m^3·s^{-1}; analyses of time series of water precipitation, flow rate and hydraulic head [Ladouche et al., 2014] emphasize the relatively inert behaviour of the system with respect to the infiltration of rain, since its characteristic time constant is on the order of 100 days.

A few records of the water temperature at the end of the spring (i.e. in the conduit itself) are available before the development of the underground pumping factory in 1982 [Lacas, 1976]: the average temperature was around 15 °C with a slight seasonal variation: the temperature was nearing 17 °C during low-water summer and tending toward lower values of about 14.5 °C following strong rain episodes. With the new technical development of the spring tapping and pumping system, hourly records of the pumped water are now available from 2006 on; it appears that the temperature of the pumped water does still vary between 14.5 °C and 17 °C and is clearly anti-correlated with the pumped flow rate. For the present study, possible artificial effects associated with the recent technical developments are ignored and the period around 1980 is chosen as reference one, when most of the present data were acquired. For this time, the mean annual temperature of the discharging spring is estimated to 15.75 °C.

In order to obtain an energy budget of the karstic system, it is also necessary to assess the input temperature of the rain water. Meteorological observations are available at several locations of the watershed area [Thiery et al., 1983] providing monthly averages of precipitation and temperature. The average annual surface temperature is somewhat dependent on the altitude of the station varying from 14 °C in its lower part (altitude 65 m) to 12.5 °C in its upper one (altitude 200 m). The Valflaunes meteorologic station (altitude 135 m, station labelled "v" on Figure 2) located in the centre of the watershed has an average annual surface temperature of 13.5 °C. Taking into account the fact that most rainy events occur during equinoxes, the average temperature of the rain is assumed to be equal to that of this later representative station (i.e. 13.5 °C). Another argument in favour of this choice is obtained from vertical profiles of temperature obtained in near surface boreholes of the area: as shown by Touet [1985], when vertical temperature profiles in the 30–100 m depth range can be extrapolated toward the ground surface, the extrapolated ground surface temperatures lies in the range (12.75 °C–13.8 °C). A value of 13.5 °C is therefore assumed to be the average temperature of the ground surface (soil + water).

In conclusion, the average discharge temperature of the spring T_{disch} = 15.75 °C is 2.25 °C higher than the assumed rain temperature (average T_{input} = 13.5 °C). Taking into account the average flow rate of the spring (q = 2 m^3·s^{-1}), this implies that during its underground path the water flow has been receiving a mean energetic input E_{spring} given in watts (W) by: $E_{\text{spring}} = (\rho C)q(T_{\text{disch}} - T_{\text{input}}) = 4.18 \times 10^6 * 2.25 * 2$ W = 18.8×10^6 W = 18.8 MW, where (ρC) is the volumetric heat capacity of water. It is reasonable to assume that this heat exchange process occurs at steady state. Obviously this energetic contribution is mainly provided by the geothermal heat flux.

2.3. *Deep regional geothermal heat flow*

Over continents, heat flow data are generally obtained from temperature profiles measured in boreholes with a few hundreds of m depth; in particular, heat flow maps of France [Lucazeau and Vasseur, 1982, Bonte and Guillou-Frottier, 2006] show that the area of southern Languedoc is characterized by a regional heat flow of 80 to 90 mW·m^{-2}. An essential condition for obtaining significant heat flow data is to avoid areas where heat convection occurs through active water flow; this precludes the use of such temperature profiles in karstic areas. However in most sedimentary basins, the oil industry has been drilling very deep boreholes for hydrocarbon exploration, reaching depths (several km) where active hydraulic fluxes are certainly much smaller; bottom hole temperatures (BHT) are recorded during well-log acquisition, being imposed more by technical purposes than by scientific ones. These rough BHT data suffer of biases reaching 5 to 15 °C due to thermal perturbations during the drilling operations but these data can be corrected leading to a set of un-biased but noisy temperatures [Vasseur et al., 1985].

A recent compilation of these data pertaining to the Provence basin (South-East of France) has been published showing a relatively consistent pattern of the deep temperature field [Garibaldi et al., 2010, Garibaldi, 2010]. For the present study, the analysis is focused on the western part of the Provence basin, i.e. west of 5 °E longitude and illustrated in Figure 3. The location of used wells (111 BHT data of which 89 at depth larger that 1000 m) is shown on Figure 3 together with a scatter plot of obtained temperatures versus depth on Figure 4. There is a clear linear increase of the temperature as a function of depth. The standard deviation (SD) of the departures between the linear fit and the data reach about 14 °C. The coefficients of the best square linear fit, with their SD writes as:

$$T(z) = 13.5 \text{ (s.d. } 0.9) \text{ °C} + 0.0318 \text{ (s.d. } 0.001)\, z \text{ (m)}. \quad (1)$$

The value at the earth surface (13.5 ± 0.9 °C) agrees with the one previously estimated.

Figure 4 also presents the temperature versus depth plot for a more localized area covering the immediate vicinity of the catchment zone and implying a smaller number of data (14 BHT). When compared to the previous linear trend, most data plot at a significantly lower temperature; indeed the regression of these data gives the following linear trend:

$$T(z) = 2 \text{ (s.d. } 3.1) \text{ °C} + 0.0.0304 \text{ (s.d. } 0.004)\, z \text{ (m)} \quad (2)$$

pointing out a consistent slope but a smaller ground surface temperature that the whole data set. This offset of about 11 °C between the extrapolated ground temperatures of these two sets of data appears significant.

It is clear that a mean regional gradient ($\gamma = \mathrm{d}T/\mathrm{d}z$) of 0.031 °C·m^{-1} (or in practical units 3.1 °C/100 m) applies to deep temperatures in the zone of interest. With such a gradient, the regional basal heat flow—based on the assumption that conduction is dominating at great depth—can be evaluated as $K\mathrm{d}T/\mathrm{d}z$ where K is the average thermal conductivity. The formations encountered in the various boreholes are mainly composed of carbonates and dolomites of Jurassic and Cretaceous age. The thermal conductivity K of such rocks can be evaluated from its composition and porosity; following Brigaud and Vasseur [1989] a value $K = 2.75 \pm 0.5$ W·°C^{-1}·m^{-1} is assessed. Assuming that conduction dominates at depth at this regional scale, these values imply a regional heat flow $K\mathrm{d}T/\mathrm{d}z$ of about 85×10^{-3} W·m^{-2} in agreement with available heat flow maps of France [Lucazeau and Vasseur, 1982, Bonte and Guillou-Frottier, 2006].

Over the catchment area (~250 km^2), the integrated energy from this geothermal flux is:

$$E_{\text{geoth}} = 0.085 \text{ W·m}^{-2} * 250 \text{ km}^2 = 21.25 \times 10^6 \text{ W} = 21 \text{ MW}. \quad (3)$$

To within experimental errors, this is very close to the mean energy E_{spring} needed for heating the spring which was estimated above from independent data. Assuming steady state conditions, everything happens as if the geothermal flux was completely absorbed for heating the water flowing in the upper crust of the Earth and emerging at the Lez spring. This absorption can indeed be verified experimentally through available temperature profiles observed in shallow wells.

2.4. *Shallow temperature gradients at basin scale*

Many temperature profiles in relatively shallow boreholes of the studied area have been obtained in the

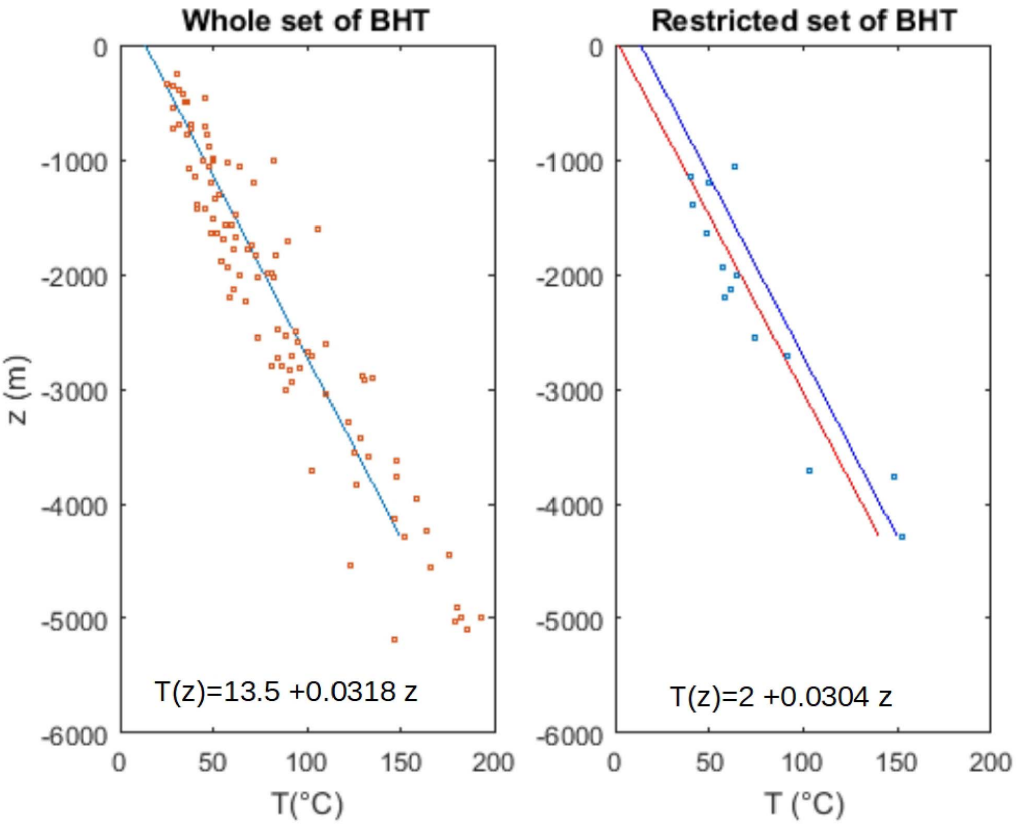

Figure 4. Plot of the measured BHT temperature versus their measurement depth (z) and best linear fitting lines. The left plot is for the whole area of Figure 3 and the blue line for best fit has equation $T(z) = 13.5\ °C + 0.0318z$. The right plot deals with the restricted area of the inset of Figure 3 and the fitting line $T(z) = 2\ °C + 0.0.0304z$, in red, is compared with the previous one of the whole area, in blue.

80s: Uil [1978], then Botton [1984] and Drogue [1985] obtained measurements in several boreholes 60 m deep located in the immediate vicinity of the spring. A wide survey at large scale was provided by Touet [1985] from high precision temperature profiles in several superficial boreholes 50 to 200 m deep located in various parts of the catchment. Most of these profiles have reached the homo-thermic zone (where seasonal effects are very small) and many of them present a clear linear trend as a function of depth. However some of these temperature profiles reflect local disturbances due to local fluid flow such as spikes due to occasional fast fluid flow across boreholes that are easily recognizable, or to flow along boreholes between two levels that is more difficult to detect.

A careful examination of these profiles allows sorting out those temperature profiles which present a regular linear trend versus depth—excluding profiles with spikes indicating lateral water arrival [Ge, 1998, Vasseur et al., 2002]. Moreover these profiles should exhibit an extrapolated ground surface consistent with meteorological data. About 17 thermal profiles have been retained, the location of which is illustrated on Figure 5 together with their geological background and two interpreted seismic cross sections of the area. Figure 6 displays seven of these profiles obtained in 1983 by Touet [1985]. The temperature gradients are all lower than 3 °C/100 m (from 0 to 2.9 °C/100 m) with a mean value on the order of 1.2 °C/100 m; from their geographic distribution, it seems that smaller values (less that 0.9 °C/100 m) are obtained toward the centre and western part of the catchment whereas higher values (near 2 °C/100 m

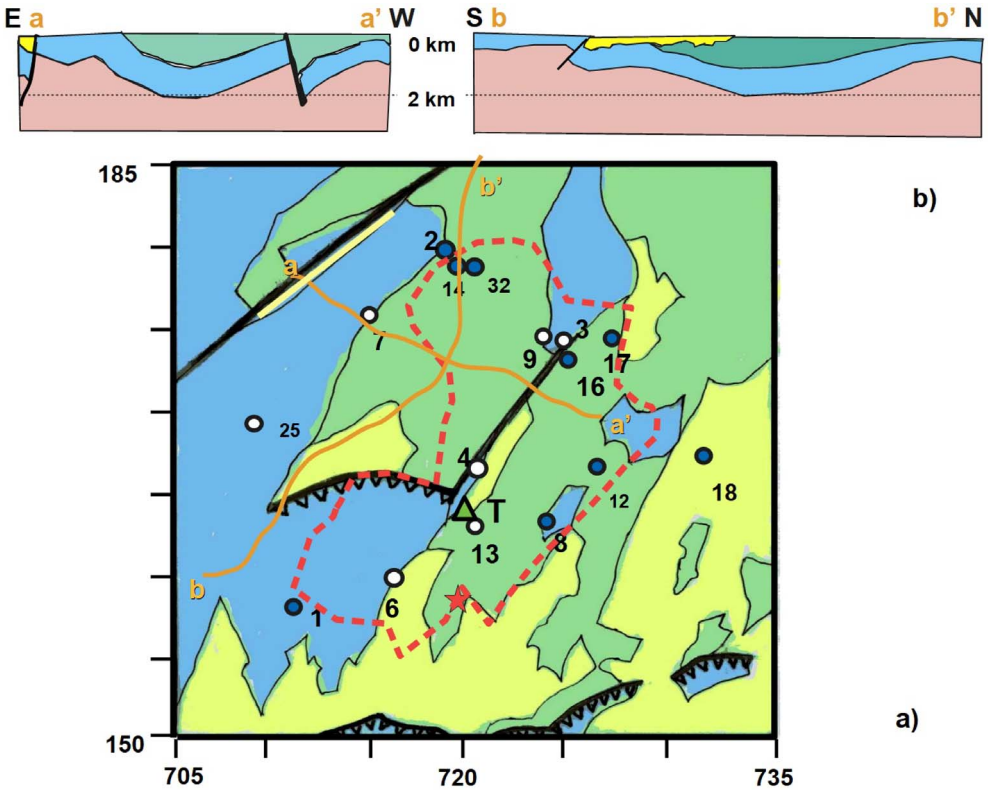

Figure 5. (a) Location of near surface thermal gradient data [Touet, 1985] in their geological context [CERGH, 1978]. The colour code is the same as for Figure 2. The Lez spring and the limit of the basin are shown in red and the dots represent the location of individual thermal gradients with their label. Open symbol are for thermal gradient <1 °C/100 m and filled ones for >1 °C/100 m. The triangle T is the location of Terrieu. Orange lines a–a′ and b–b′ correspond to available seismic profiles. (b) Two cross sections along approximate NS and EW directions obtained from migrated seismic data as interpreted by Husson [2013].

or above) are observed toward its northern, eastern and southern edges. A trend analysis of these data, fitted with a polynomial of second degree in x and y as shown on Figure 7 confirms this trend: a zone of depleted gradient occurs toward the centre of the recharge zone.

3. A simplified model of karst circulation

Based on the scheme described on Figure 1, a simplified model is designed where the karstic conduit, simulated by a horizontal fracture, is embedded in a porous medium simulating the fractured medium. This model, illustrated by Figure 8, reduces the problem to a pseudo 2-dimensional one and allows a simple analytical solution. Notations are summarized in Table 1.

3.1. *Basic assumptions*

The reference frame illustrated on Figure 8 is such that Oxy is the ground surface assimilated to the water table, Oz the downward vertical, and Ox the horizontal direction parallel to that of the water flow inside the conduit. In the porous rock matrix ($0 < z < h$), the porous water flow is characterized by the downward component of the specific discharge $\vec{V}$ and its temperature T is in equilibrium with that of the rock.

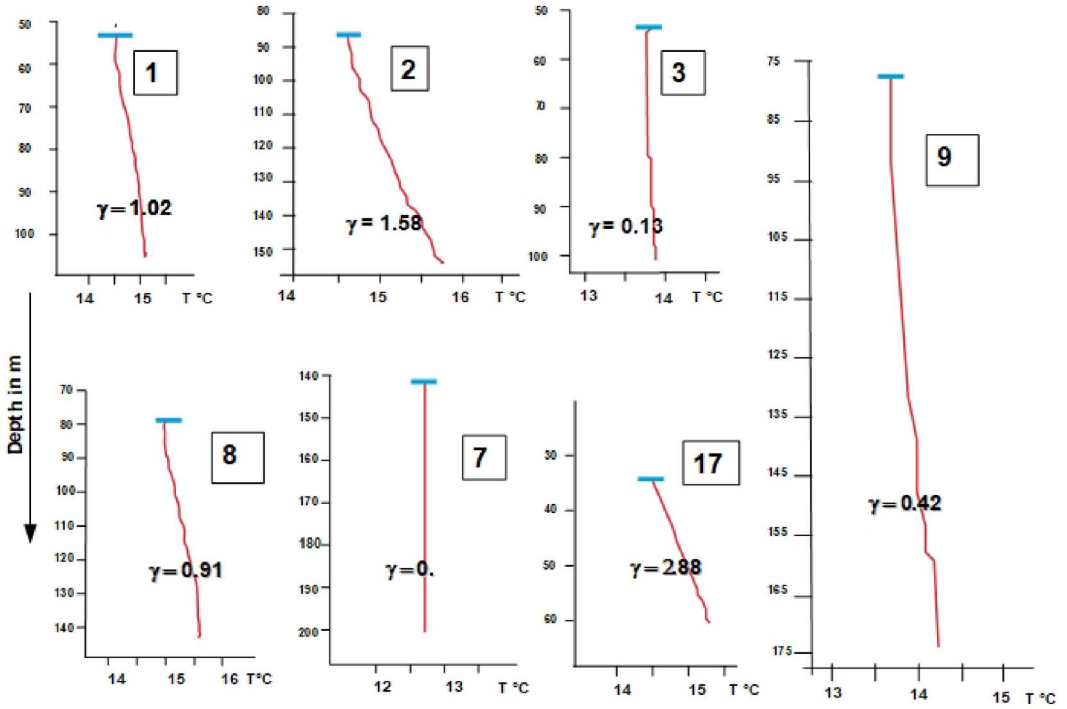

Figure 6. Illustration of seven typical near surface thermal profiles with corresponding thermal gradient $\gamma = \mathrm{d}T/\mathrm{d}z$ in °C/100 m. The profiles measured in 1983 are redrawn in red from Touet [1985]. The ordinate is the depth from the ground surface; the level of the water table is shown as a blue line and the number in square inset correspond to the label located on Figure 5.

The thermal energy is transported by conduction in the porous medium with an energy flux given by—K grad T (K being the thermal conductivity of the porous medium) and also by convection of the moving fluid. The total energy per unit mass transported by this moving fluid is composed of its thermal energy written as CT (C the heat capacity per unit mass) plus other types of energy: internal fluid pressure, kinetic energy and potential energy. The necessary introduction of gravity potential in the total energy budget of porous flow has been pointed out in several theoretical studies [Sposito and Chu, 1981, Hassanizadeh and Gray, 1980]. More recently Stauffer et al. [2014]—see also Burns et al. [2016]—have enlightened the subject in practical applications; following Stauffer et al. [2014], the methalpy θ sums up the specific enthalpy $e = CT + p/\rho$ (p being the fluid pressure, ρ its density) plus its kinetic energy $V^2/2$ (in fact negligible in porous media) and finally its potential energy due to its evolution in the gravity potential i.e. $-gz$ (z being directed downward). The methalpy is defined by:

$$\theta = CT + \frac{p}{\rho} + \frac{V^2}{2} - gz. \tag{4}$$

Assuming that the solid phase of the porous medium is rigid and in thermodynamic equilibrium with the fluid, the principle of energy conservation at steady state [Stauffer et al., 2014, Burns et al., 2016] implies that the divergence of the conductive flux $-K\mathrm{grad}(T) = -K\vec{\nabla}T$ in the porous plus the divergence of the convective flux of θ is 0:

$$\begin{aligned} 0 &= \mathrm{div}(-K\vec{\nabla}T + \rho\theta\vec{V}) \\ &= -K\Delta T + (\rho C)\vec{V}\cdot\vec{\nabla}T + \vec{V}\cdot\vec{\nabla}(p - \rho gz) \end{aligned} \tag{5}$$

where ΔT is the Laplacian of T (i.e. div(grad (T))). For obtaining the last right hand side (rhs) of (5), use was made of the fact that div($\vec{V}$) = 0 (from fluid mass

Table 1. List of used symbols

Symbol	Significance	Unit
C	Heat capacity of the water per unit mass	$\mathrm{J{\cdot}kg^{-1}{\cdot}{^\circ}C^{-1}}$
E	Energy output	W
EE	Function defined by $EE(u) = \mathrm{erfc}(u)\exp(u^2)$	
F_S	Conductive heat flow at the ground surface	$\mathrm{W{\cdot}m^{-2}}$
$G = g/C$	Thermal gradient associated with gravitational potential dissipation	$\mathrm{{^\circ}C{\cdot}m^{-1}}$
H	Hydraulic head $= p/(\rho g) - z$	m
K	Thermal conductivity of porous medium	$\mathrm{W{\cdot}m^{-1}{\cdot}{^\circ}C^{-1}}$
L	Length of the conduit (x direction)	m
Pe	Peclet number	
R	Radius of a horizontal disk	m
S_f	Shape factor	m
$T(x,z), T^+, T^-$	Temperature field in the porous medium, above h, below h	°C
$T_0, T_{\mathrm{ground}}, T_{\mathrm{extrap}}$	Temperature in the conduit of the ground and extrapolated	°C
V	Specific discharge in z direction. Eventually vector (Darcy vel.).	$\mathrm{m{\cdot}s^{-1}}$
e	Specific enthalpy $e = CT + p/\rho$	$\mathrm{J{\cdot}kg^{-1}}$
g	Acceleration of gravity ($g = 9.81$)	$\mathrm{m{\cdot}s^{-2}}$
h	Depth of the conduit	m
q	Horizontal flux in the x direction per unit y	$\mathrm{m^2{\cdot}s^{-1}}$
x	Horizontal coordinate along the flow	m
y	Horizontal coordinate perpendicular to x	m
t	Time	s
z	Vertical coordinate orientated downward	m
α	Vertical gradient of H	m/m
β	Horizontal gradient of H	m/m
ε	Thickness of the conduit	m
γ	Geothermal gradient	$\mathrm{{^\circ}C{\cdot}m^{-1}}$
ρ	Density of water	$\mathrm{kg{\cdot}m^{-3}}$
κ	Diffusivity of the porous medium $(\rho C)_r/K$	$\mathrm{m^2{\cdot}s^{-1}}$
θ	Specific methalpy $\theta = e - gz$	$\mathrm{J{\cdot}kg^{-1}}$
(ρC)	Volumetric specific heat of water	$\mathrm{J{\cdot}kg^{-1}{\cdot}{^\circ}C^{-1}}$
$(\rho C)_r$	Volumetric specific heat of medium, of water	$\mathrm{J{\cdot}kg^{-1}{\cdot}{^\circ}C^{-1}}$
$\tau_{\mathrm{diff}}, \tau_{\mathrm{conv}}$	Time constant for diffusion, convection	s

conservation) and the kinetic term of θ was omitted as negligible. The first term of the rhs arises from conduction, the second from water convection transporting internal heat and the last term acts as a source term which accounts for the transport of pressure and gravity potential variations. This last term is usefully expressed as a function of the hydraulic head arbitrarily defined with respect to the ground level $z = 0$:

$$H = \frac{p}{\rho g} - z. \tag{6}$$

The head H, i.e. the potential (in m) associated with the dynamics of porous flow through the Darcy law, is thus the relevant quantity for including the effect of gravity potential and pressure in the energy budget. The coupling of these two items is not astonish-

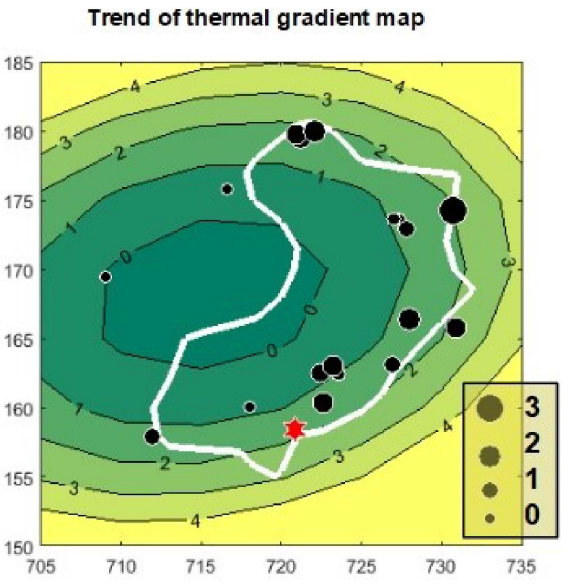

Figure 7. The large scale trend of the surface thermal gradient fitted by a polynomial surface of second degree in latitude–longitude on the same area as Figure 6. The values are in °C/100 m and the position of individual data is illustrated by dots. The size of dots is proportional to their value according to the bottom right legend (in °C/100 m).

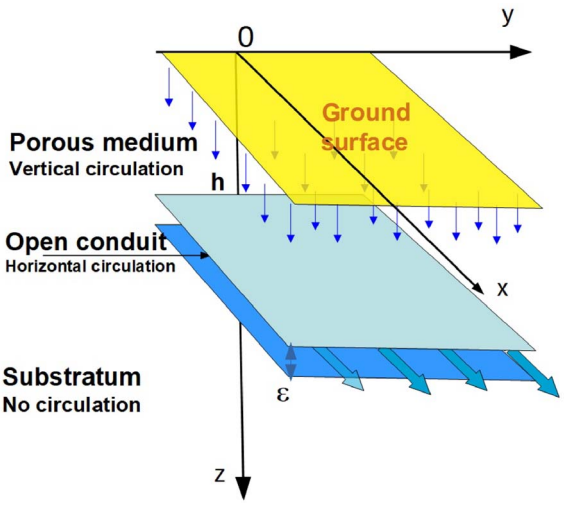

Figure 8. Simplified geometry of the model used; the reference frame is Oxyz, Oz being the downward vertical, Oxy the ground plane (yellow) and Ox the direction of the conduit flow. The conduit is a thin horizontal fault of thickness ε at $z = h$. The water fluxes, illustrated by blue arrows, are vertical in the surrounding porous medium; they converge into the conduit to follow the Ox direction.

ing since variations of p/ρ can be seen as the internal response to variations of the altitude z. (This is opposite to a previous proposition of the author, who neglected the pressure term in (5); he was obviously wrong.)

Therefore, in the whole porous domain, the energy conservation in steady state conditions is expressed as:

$$K\Delta T - (\rho C)\vec{V}\cdot\vec{\nabla}T - (\rho g)\vec{V}\cdot\vec{\nabla}H = K\Delta T - (\rho C)\vec{V}\cdot\vec{\nabla}T - (\rho C)G\vec{V}\cdot\vec{\nabla}H = 0 \quad (7)$$

where G was introduced as the useful parameter:

$$G = g/C. \quad (8)$$

As seen from (7) this parameter G has a dimension of a temperature gradient and its value is 9.8 m·s^{-2}/4180 J·kg^{-1}·°C^{-1} = 0.0023 °C·m^{-1}. G is much smaller that the classical geothermal gradient γ which is in the order of 3 °C per 100 m.

At depth $z = h$, as shown on Figure 8, lies a conduit assimilated to a "horizontal feature" with vertical thickness ε ($\varepsilon \ll h$). This feature is in fact associated with a hydraulically conductive structure which is stretched in the x, y directions. It could even be a thin aquifer much more conductive that the overlying medium; in the following it is referred to as "plane conduit". Inside this conduit, the horizontal water flow $q(x)$ is the cumulative result from the downward flow occurring in the overlying porous medium (vertical component V along coordinates z). At steady state, mass conservation imposes that the vertical specific discharge (Darcy velocity) is related to the increase along x of the water flow rate q (in m^2·s^{-1} i.e. per unit length in the y direction) so that q and V are related by:

$$V = \frac{\mathrm{d}q}{\mathrm{d}x}. \quad (9)$$

A further approximation is that the horizontal conduction along the direction can be neglected since horizontal gradients are much smaller that vertical ones; nevertheless, the problem remains a 2D one

because thermal coupling along Ox is realized by the cumulative flow of heat and mass into the conduit. By hypothesis T does not depend on y and is written as $T(x,z)$.

In the porous medium located above the conduit ($z<h$), the temperature field indexed as $T^+(x,z)$ is submitted to the downward water flow and from (7) satisfies the following equation:

$$\text{for } 0<z<h \quad K\frac{\partial^2 T^+}{\partial z^2}-(\rho C)V\frac{\partial T^+}{\partial z}-(\rho C)VG\frac{\mathrm{d}H}{\mathrm{d}z}=0 \tag{10}$$

whereas, deeper than the conduit ($z>h$), conduction is the only mechanism. There, the temperature field, indexed as $T^-(x,z)$ satisfies:

$$\text{for } z>h \quad \frac{\partial^2 T^-}{\partial z^2}=0. \tag{11}$$

Classical boundary conditions include imposed temperature at the ground surface (arbitrarily set to 0) and imposed vertical gradient γ (or given geothermal heat flux $\varphi_{\text{geoth}}=K\gamma$) at great depth, so that:

• at $z=0$

$$T^+(x,0)=0 \tag{12}$$

• at $z=+\infty$

$$\frac{\partial T^-}{\partial z}(x,+\infty)=\gamma. \tag{13}$$

At the level $z=h$, two specific boundary conditions are required: one accounts for the continuity of the temperature and the other for a possible discontinuity of its derivatives accounting for the energy conservation in the conduit. Since the thickness ε is very small, the temperature above and below are continuous (but not their vertical derivatives) so that:

• at $z=h$

$$T^+(x,h)=T^-(x,h)=T_0(x) \tag{14}$$

where T_0 is the temperature of the conduit. The fourth condition stems from the energy budget at the conduit level and involves not only the convective and conductive heat flow but also the pressure and gravity potential of the fluid phase. This is obtained using the surface integral equivalent of the energy conservation (7). For a volumetric element ($\mathrm{d}x\,\mathrm{d}y\varepsilon$) of the plane conduit (Figure 9), the input of conductive plus convective energy including methalpy is 0 for steady state conditions:

• at $z=h$

$$\begin{aligned}0=&-K\frac{\partial T}{\partial z}\bigg|_-^+-(\rho C)\frac{\mathrm{d}(qT_0)}{\mathrm{d}x}+(\rho C)VT_0\\&-(\rho C)G\frac{\partial(qH)}{\partial x}\bigg|_{z=h}+(\rho C)GVH|_h\\=&-K\frac{\partial T}{\partial z}\bigg|_-^+-(\rho C)q\frac{\mathrm{d}T_0}{\mathrm{d}x}-(\rho C)Gq\frac{\partial H}{\partial x}.\end{aligned} \tag{15}$$

Immediately to the right of the sign "0 =", the first term containing the discontinuity of temperature gradient at $z=h$ is the net conductive heat flow from above and below; the second and third terms are the convective heat input respectively in the horizontal direction and in the vertical one and the fourth and fifth ones the corresponding contributions of fluid pressure and gravity potential (both included in the head H). The horizontal conductive term is omitted because it is negligible with respect to the horizontal convection. The simplification leading to the final expression arises from the relation $V=\mathrm{d}q/\mathrm{d}x$.

Since steady state is assumed, the energy budget of the conduit element equal to 0 provides the fourth boundary condition as (15). This boundary condition seems quite similar to the one stated by Bovardsson [1969], Lowell [1975], Ziagos and Blackwell [1986] for the case of a horizontal aquifer. In fact it differs because the energy contains more than internal heat as already stated by Burns et al. [2016]. But the main difference is that horizontal water flux $q(x)$ is not constant with x: it is accumulating the water flux supplied vertically by the porous flow.

In the next paragraphs useful analytical solutions are obtained for cases where the parameters $\alpha=-\mathrm{d}H/\mathrm{d}z$ in the porous medium, and $\beta=-\mathrm{d}H/\mathrm{d}x$ in the horizontal conduit are assumed to be constant on the whole domain. Both parameters α, β are related the dynamics of the underground water flow along the path. Since the flow is orientated downward and toward the spring, α and β are strictly positive; This implies that $-\mathrm{d}H/\mathrm{d}s$ (i.e. α, β) acts as a positive energy contribution in (15). Moreover they belong to the range $[0,1]$; whenever α or β are very small, the variations of fluid pressure p are nearly compensating those of the gravity potential $\rho g z$; H is then nearly constant along the water flow lines i.e. hydraulic equilibrium is nearly satisfied and the head contribution to the energy budget vanishes. On the contrary, when α increases toward 1, the gradient of fluid pressure decreases with respect to that of the

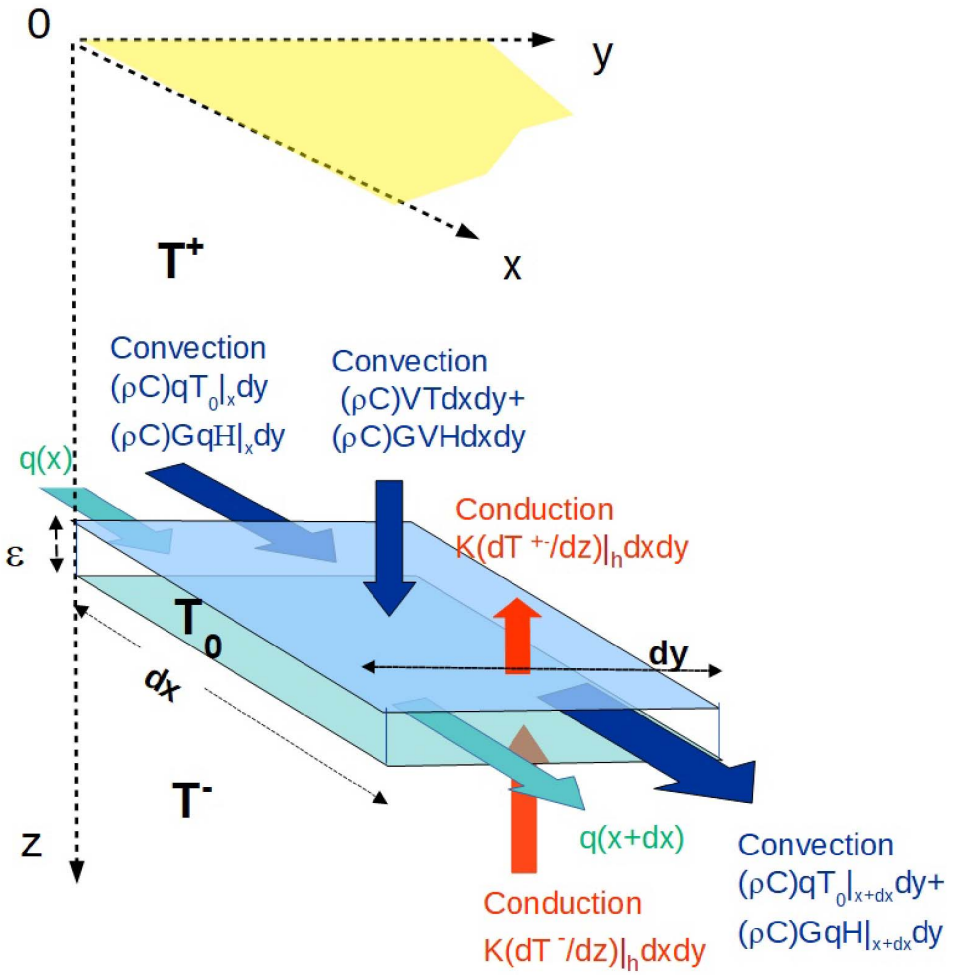

Figure 9. Budget of mass and heat transfer in an elementary cell of the conduit illustrating the various components: the water fluxes are shown in light blue, the convective fluxes of heat content $(\rho C)T$ and gravity-head potential $\rho g H$ in dark blue and the conducting fluxes in red.

gravity potential (then constant and =1) and its contribution to the energy budget is then maximum.

The Equation (10) with conditions given by (11)–(13) can be solved with z as a function of the parameter $T_0(x)$. It is of common practice to introduce a local Peclet number, which characterizes the importance of convection with respect to conduction as defined by:

$$Pe(x) = \frac{(\rho C)V(x)h}{K}. \tag{16}$$

Mathematically the problem is to solve the system:

$$\text{For } 0 < z < h \quad \frac{\partial^2 T^+}{\partial z^2} - \frac{Pe}{h}\frac{\partial T^+}{\partial z} + \frac{PeG\alpha}{h} = 0 \tag{17}$$

$$\text{for } z > h \quad \frac{\partial^2 T^-}{\partial z^2} = 0 \tag{18}$$

with boundary conditions given by (12)–(14). Let's replace for the moment the fourth condition by $T^+(x,h) = T^-(x,h) = T_0(x)$; the solution of (17) is obtained as a function of $T_0(x)$:

$$T^+(x,z) = \frac{T_0(x) - G\alpha h}{\exp(Pe) - 1} * \left(\exp\left(\frac{Pez}{h}\right) - 1\right) + G\alpha z. \tag{19}$$

Similarly, that of (18) with boundary condition (14) is:

$$T^-(x,z) = T_0(x) + \gamma(z-h). \tag{20}$$

These two solutions are continuous at the level of the conduit $z=h$: i.e. $T^+(x,z=h) = T^-(x,z=h) = T_0(z)$. However their derivatives are discontinuous so that the jump of conductive flux at $z=h$:

$$K\frac{\partial T}{\partial z}\bigg|_{-z=h}^{+} = K\left[\frac{Pe}{h}\frac{T_0 - G\alpha h}{\exp(-Pe)-1} - G\alpha + \gamma\right]. \tag{21}$$

Applying the fourth boundary condition, i.e. the energy budget described by (15) leads to the following equation for T_0:

$$\frac{(\rho C)V}{K}\frac{(T_0 - G\alpha h)}{1-\exp(-Pe)} - \gamma + G\alpha + \frac{(\rho C)q}{K}\frac{\mathrm{d}(T_0 - G\beta x)}{\mathrm{d}x} = 0 \tag{22}$$

which can also be written as:

$$\begin{aligned}&\frac{(\rho C)V}{K}\frac{(T_0 - G\alpha h - G\beta x)}{1-\exp(-Pe)}\\ &\quad + \frac{(\rho C)q}{K}\frac{\mathrm{d}(T_0 - G\alpha h - G\beta x)}{\mathrm{d}x}\\ &\quad = \gamma - G\alpha - \frac{(\rho C)V}{K}\frac{G\beta x}{1-\exp(-Pe)}.\end{aligned} \tag{23}$$

This is a first order differential equation for $T_0(x)$ which can solved analytically in two specific cases of interest, depending on the assumption on $V(x)$ (therefore $q(x)$ and $Pe(x)$).

3.2. $Pe(x)$ *is* $\gg 1$ *in the entire domain of infiltration*

Now, consider that the domain where vertical infiltration occurs is limited from $x=0$ to $x=L$ so that $q(0)=0$ and $q(L)$ is the final outflow rate. Let assume that in this range of x value, $Pe(x)$ is large enough so that $\mathrm{e}^{-Pe(x)} \ll 1$ (in practice $Pe>3$), then the lhs of (23) can be modified to highlight a primitive:

$$\begin{aligned}&\frac{(\rho C)V(x)}{K}\left(T_0 - G\alpha h - G\beta x\right)\\ &\quad + \frac{(\rho C)q(x)}{K}\frac{\mathrm{d}(T_0 - G\alpha h - G\beta x)}{\mathrm{d}x}\\ &\quad = \gamma - G\alpha - G\beta\frac{(\rho C)V(x)x}{K}.\end{aligned} \tag{24}$$

It can be integrated from $x=0$ (where $q(0)=0$) to L leading to:

$$\begin{aligned}&\frac{(\rho C)q(L)}{K}(T_0 - G\alpha h - G\beta L)\\ &\quad = (\gamma - G\alpha)L - \frac{(\rho C)}{K}G\beta\int xV(x)\mathrm{d}x\end{aligned} \tag{25}$$

or:

$$T_0(L) = G\alpha h + G\beta(L - L_b) + \frac{(\gamma - G\alpha)h}{\langle Pe\rangle_L} \tag{26}$$

where L_b denotes the barycentre of the infiltration velocity ($=L/2$ when V is homogeneous) and $\langle Pe\rangle_L$ the average Peclet number over the range $(0, L)$ both defined by:

$$\langle Pe\rangle_L = \frac{(\rho C)h}{K}\frac{q(L)}{L} \quad L_b = \frac{\int xV\mathrm{d}x}{q(L)}. \tag{27}$$

These results can be applied for any $x<L$ when replacing in (26)–(27) L by x.

3.3. $Pe(x)$ *remains constant in the entire domain of infiltration*

Assuming that V (and so Pe) remains constant with x (without restriction on its value), the first order differential equation has a particular solution which writes:

$$\begin{aligned}T_0(x) = G\alpha h + \frac{(\gamma - G\alpha)h}{Pe}(1-\exp(-Pe))\\ + G\beta\left(\frac{1-\exp(-Pe)}{2-\exp(-Pe)}\right)x.\end{aligned} \tag{28}$$

From (16)–(17) it corresponds to the vertical profile of temperature:

$$\begin{aligned}T^+(x,z) = &\left(\frac{(\gamma - G\alpha)h}{Pe} + \frac{G\beta x}{2-\exp(-Pe)}\right)\\ &\times\frac{\exp(Pez/h)-1}{\exp(Pe)} + G\alpha z \quad \text{for } z<h\end{aligned} \tag{29}$$

$$\begin{aligned}T^-(x,z) = &G\alpha h + \frac{(\gamma - G\alpha)h}{Pe}(1-\exp(-Pe))\\ &+ G\beta\left(\frac{1-\exp(-Pe)}{2-\exp(-Pe)}\right)x + \gamma(z-h) \quad \text{for } z>h.\end{aligned} \tag{30}$$

The resulting solution $T(x,z)$ is illustrated in non-dimension units ($T/\gamma h$ and z/h) on Figure 10a omitting its linear variation in x (i.e. $\beta=0$): vertical profiles of temperature are presented for various values of Pe. A comparison of $T(\cdot,z)$ profiles obtained with $\alpha=0$ with those obtained with $\alpha=0.5$ illustrates the relatively small but substantial effect of this last parameter. The profile bending at $z=h$ can be characterized by the intercept of the linear trend of the deep temperature $T^-(x,z)$ when extrapolated at $z=0$:

$$\begin{aligned}T_{\mathrm{extrap}}(x) = T_0(x,0) - \gamma h = G\alpha h\\ + \frac{(\gamma - G\alpha)h}{Pe}(1-\exp(-Pe))\\ + G\beta\left(\frac{1-\exp(-Pe)}{2-\exp(-Pe)}\right)x - \gamma h.\end{aligned} \tag{31}$$

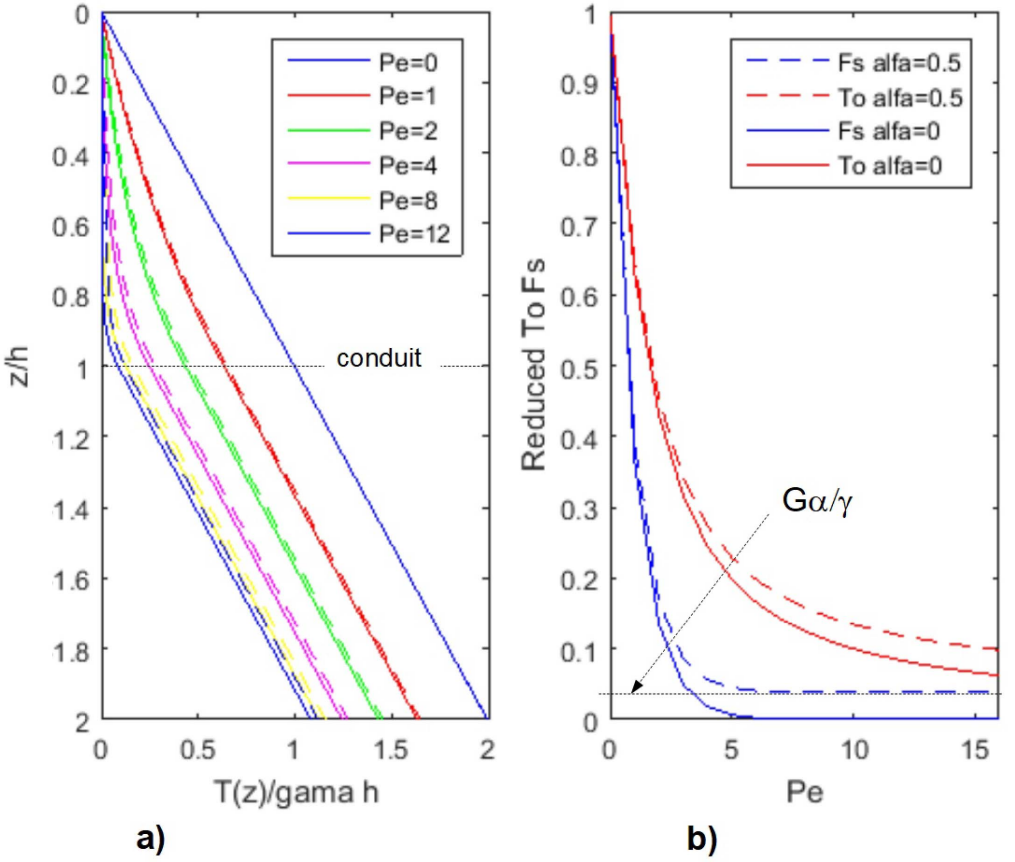

Figure 10. (a) Normalized temperature ($T/\gamma h$) versus normalized depth (z/h) for the plane conduit model in the established regime for various values of Pe and 2 values of α. For emphasizing the effect of gravity-head potential, a strong value of α (0.5) is chosen. Continuous lines are for $\alpha = 0$ and dotted ones for $\alpha = 0.5$ (i.e. $G\alpha/\gamma = 0.039$). (b) Corresponding value of the normalized conduit temperature T_0 ($T_0/\gamma h$) and of the normalized surface heat flow F_S ($\mathrm{d}T/\mathrm{d}z/\gamma$). Continuous lines are for $\alpha = 0$ and dotted ones for $\alpha = 0.5$ (i.e. $G\alpha/\gamma = 0.039$).

At the ground surface, the "residual" conductive heat flow F_S is:

$$F_S = K\frac{\partial T}{\partial z}\bigg|_{z=0} = K\gamma\exp(-Pe) + KG\alpha(1-\exp(-Pe)) + KG\beta\frac{x}{h}\frac{Pe\cdot\exp(-Pe)}{(2-\exp(-Pe))}. \quad (32)$$

The first term of the rhs is the deep geothermal heat flow, once attenuated by an exponential factor, the second and third ones accounts for the gravitational effect during the downward infiltration the final horizontal flow. When $Pe \to \infty$ F_S (and therefore the vertical thermal gradient) does not tend toward 0 but toward a threshold given by $KG\alpha$. It can be verified from (32) that the input of thermal energy for heating water from its initial temperature $T = 0$ at the surface to its value $T_0(x)$ along the conduit is equal to the bottom heat flow minus the residual surface heat flow plus two components associated with gravity effects: the first is associated with the vertical path and the second one to the horizontal path as shown below:

$$\begin{aligned}(\rho C)VT_0 &= \frac{(\rho C)Vh}{Pe}(\gamma - G\alpha)[1-\mathrm{e}^{-Pe}] + (\rho C)VG\alpha h \\ &\quad + (\rho C)VG\beta\frac{(1-\mathrm{e}^{-Pe})}{(2-\mathrm{e}^{-Pe})}x \\ &= K\gamma - F_S + (\rho C)VG\left[\alpha h - \frac{\beta x}{2-\mathrm{e}^{-Pe}}\right]. \quad (33)\end{aligned}$$

Figure 10b depicts how T_0 and F_S depends on Pe; the x dependence is omitted (i.e. $\beta = 0$) and both quantities are normalized to their undisturbed values γh

(for temperature) and $K\gamma$ (for flux); the role of the gravity potential component is illustrated by comparison of two values either $\alpha = 0$ and $\alpha = 0.5$. Both T_0 and F_S decrease with Pe; for high Pe, T_0 and F_S tend exponentially toward a limit ($G\alpha h$ and $KG\alpha$ respectively) which becomes 0 when $\alpha = 0$.

3.4. *Case of a recharge window ($Pe = Cst$ for $0 < x < L$ and $Pe = 0$ elsewhere)*

General solutions of (23) are now investigated for the case of a recharge window ($V \neq 0$) limited to the range $x = 0$ to L as illustrated by Figure 11a. Only the case $\beta = 0$ is considered for sake of simplicity.

- for $x < 0$, $V = 0$ and the conduit is not recharged so that $q(x) = 0$; thus the standard conductive equilibrium $T(x,z) = \gamma z$ applies;
- for $0 < x < L$, water infiltration with constant V occurs; it is supplying the conduit flow resulting in a flow rate increasing linearly according to $q(x) = Vx$;
- for $x > L$, $V = 0$; for $x > L$, $q(x)$ is now constant and becomes $q(x) = VL$.

For $x < 0$, the assumed initial conduit temperature is just $T_{0\text{ini}} = \gamma h$.

For $0 < x < L$, $T_0(x)$ is solution of:

$$x\frac{\mathrm{d}(T_0 - G\alpha h)}{\mathrm{d}x} + \frac{(T_0 - G\alpha h)}{1-\exp(-Pe)} = \frac{(\gamma - G\alpha)h}{Pe}. \qquad (34)$$

The general solution of this first order differential equation is:

$$T_0(x) = G\alpha h + \frac{(\gamma - G\alpha)h}{Pe}\left[1 - \exp(-Pe)\right] + Cst\left(\frac{1}{x}\right)^{\frac{1}{1-\exp(-Pe)}} = T_0^* + Cst\left(\frac{1}{x}\right)^{\frac{1}{1-\exp(-Pe)}} \qquad (35)$$

where T_0^* is the particular temperature (28) previously described, also called established temperature. The constant Cst is defined by the boundary condition ($T_0(0) = T_{0\text{ini}} = \gamma h$) at $x = 0$. In fact, due to the singular behavior of the solution at $x = 0$, this boundary condition cannot be imposed at all. This difficulty is associated with the oversimplification of zero horizontal conduction in the whole porous medium which results in cancelling any heat sink at $x = 0$. Nevertheless it can be qualitatively overcome according to the following approximate scheme.

It is possible to avoid the singularity of the solution (35) at $x = 0$ by adding into (34) a dissipating term in the energy budget; this dissipating term accounts for horizontal conduction along x limited to a horizontal strip of half thickness $h/2$ around the conduit. The boundary condition now applies: after a few development detailed in Appendix A, for large Pe, the solution of the modified equation is now:

$$T_0(x) = T_0^* + (T_{0\text{ini}} - T_0^*)EE[\sqrt{Pe}x/h] \qquad (36)$$

where $EE(u)$ is the function given by $EE(u) = \exp(u^2)\mathrm{erfc}(u)$. $EE(u)$ is a classical function in heat transfer problems [Carslaw and Jaeger, 1959, p. 482]: it is equal to 1 for $u = 0$, behaves as $1/u$ for large u where it can be roughly approximated $1/(1 + 1.5u)$. Since $EE(u) = 1/\mathrm{e}$ for $u = 1.23$, the horizontal distance z for which $T_0(z) - T_0^* = (T_{0\text{ini}} - T_0^*)/\mathrm{e}$ is roughly $L_u \sim 2.18h/\sqrt{Pe}$. This emphasizes the rapid convergence of $T_0(z)$ toward the established regime T_0^* and especially for high Pe.

When for $z > L$, the recharge is stopped; $q(x)$ remains constant and equal to VL but the model has to be adapted. This is because, in this case, Equation (10) becomes simply $\partial^2 T^+/\partial z^2 = 0$: the vertical temperature profile is simply linear above and below the conduit. But, at the level $z = h$, the slopes of these two linear segments are different in order to compensate for the horizontal decay of the convective heat flow in the conduit. The heat budget of the conduit writes:

$$-(\rho C)q\frac{\mathrm{d}T_0}{\mathrm{d}x} - K\left.\frac{\partial T}{\partial z}\right|_-^+ = -(\rho C)q\frac{\mathrm{d}T_0}{\mathrm{d}x} - K\left(\frac{T_0}{h} - \gamma\right) = 0 \qquad (37)$$

or:

$$PeL\frac{\mathrm{d}T_0}{\mathrm{d}x} + T_0 = \gamma h \qquad (38)$$

the solution of which is:

$$T_0(x) = \gamma h + (T_{0L} - \gamma h)\exp[-(x-L)/PeL] \qquad (39)$$

with the boundary condition at $z = L$ that $T_0(L) = T_{0L}$ at $z = L$ (if $L \gg h$ for example, $T_{0L} \sim T_0^*$). Therefore, when the recharge of the conduit flow stops, its temperature returns exponentially toward the undisturbed temperature γh with a characteristic length PeL. These results, although obtained with an approximate account of lateral conduction, have been ascertained numerically with the help of numerical computations using finite differences and accounting for 2-D conduction as illustrated by Figure 11b.

The final result of this study is that, when infiltration supplying the conduit flow occurs abruptly in x, the established regime is rapidly dominant in

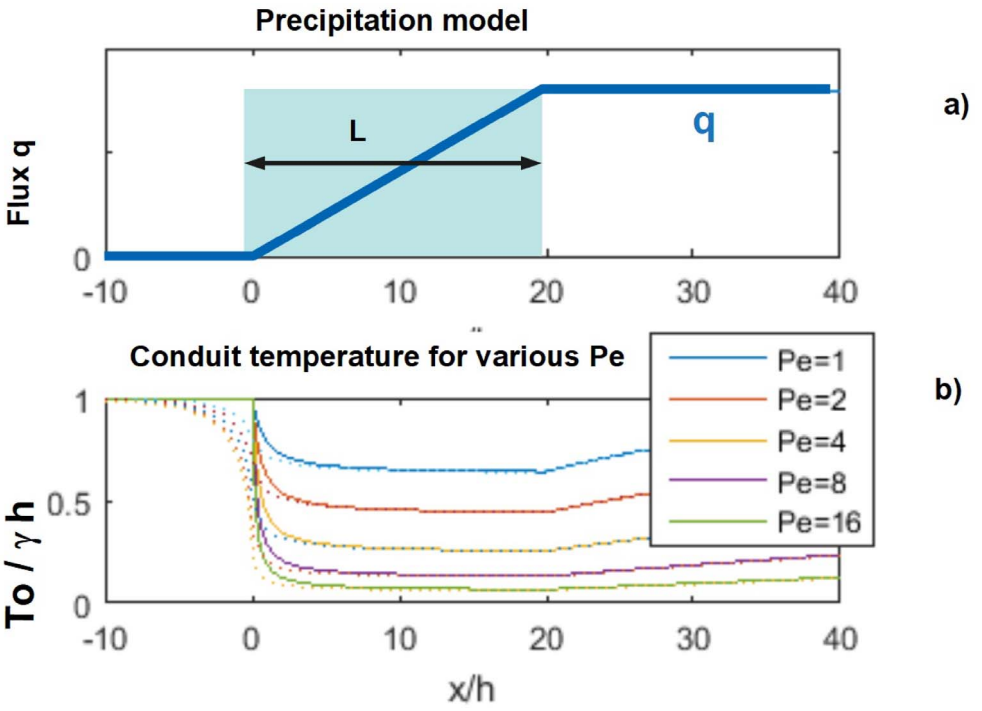

Figure 11. Cross section along x direction showing the effect of a limited infiltration ($0 < x < L = 20$ h) recharging the conduit. (a) Represents the evolution of the water flux $q(z)$ in the conduit and (b) plots the normalized conduit temperature $T_0(x)$ for several Pe values. The dotted lines show the numerical value and the full lines the approximation of (36) of Section 3.4.

x except in a narrow range of x values (on the order of $h/\sqrt{Pe}$). Also when the supply is suppressed for $x > L$, T_0 decreases exponentially with a characteristic length PeL so that this decrease in x is very slow. Furthermore the integral solution described above allows to generalize these results for varying Pe, Pe being replaced by its arithmetic average. Since in the actual case $h \ll L$ and $Pe > 1$, the practical conclusion is that the actual thermal data of T_0 can be directly compared to the prevision of the model through (26)–(28). These analytical results can now be compared to actual thermal data.

4. Application of the model to Lez data; results and discussion

The available thermal data are: (1) the temperature of the Lez spring which is identified to T_0 at the output of the system, (2) the near surface temperature gradients in shallow boreholes (Fs/K) and (3) the deep temperature trend extrapolated onto the ground surface (T_{extrap}) from oil exploration data extrapolation. Some parameters are well known constants such as $(\rho C) = 4.18 \times 10^6$ W·°C^{-1}·m^{-3}, $G = 0.23$ °C/100 m; others apply to the site (cf Section 2) such as rock conductivity $K = 2.75$ W·m^{-1}·°C^{-1}, deep geothermal gradient $\gamma = 3.1$ °C/100, length of the system $L =$ 15,000 m.

However the head gradients along the vertical path $\alpha = -\mathrm{d}H/\mathrm{d}z$ and along the horizontal paths $\beta = -\mathrm{d}H/\mathrm{d}x$ also need to be defined; in the following, their value is speculated on the basis of available piezometric data. Water level has been continuously monitored in about 20 piezometers beginning in the 1980s [Avias, 1995]. The observed difference of water levels between the upper part of the watershed and the spring is on the order of some tens of m and rarely exceeds 100 m [Karam, 1989, Avias, 1995]. This decrease of H along the water path is associated partly with the downward infiltration path (coefficient α) and partly with the horizontal path in

the conduit (coefficient β); none of them is available from actual data. In order to appreciate the importance of the gravity-head potential term on the result, two extreme assumptions will be made:

- either α, β are both 0 or at least very small i.e. a quasi hydraulic equilibrium occurs along the path; this implies no contribution to the energy transport since the gravity potential effect is fully compensated by that of the water pressure;
- or a head decrease on the order of δH = 100 m is occurring between the ground level and the spring; half of this decrease is assigned to the vertical path (α = 0.1 m/m for a vertical depth around 500 m as obtained below) and the other half to the horizontal one (β = 0.0067 m/m for a horizontal length around 15 km). The fact that $\alpha > \beta$ reflects the fact that the impedance of the conduit is obviously much smaller than that of the porous medium.

4.1. *Global parameters: use of T_0 and T_{extrapol}*

The observations of T_0 and T_{extrap} are now used in the above 1D model to derive from (26)–(31) unknown parameters. These unknown quantities are h and Pe, but since $Pe = (\rho C)Vh/K$, it is clear the actual unknowns are h and V: in practice Pe may be expressed as $Pe = 0.049\,Vh$ with h in m and V in m/year.

From the data T_0 and T_{extrap},—eventually expressed as deviations, with respect to T_{ground}—the value of h is easily computed using (31): the difference $\gamma h = T_{\text{extrap}} - T_0$ gives h = 440 m. The average value of Pe is then obtained from (26). In the case $\alpha = \beta = 0$ (26) reduces to $\langle Pe\rangle = \gamma h/T_0 = 6$. In the case α = 0.1, β = 0.01, Equation (26) leads to $\langle Pe\rangle$ = 6.8 which is significantly higher.

From these values of Pe, one can deduce the vertical specific discharge V = 0.28 m·y^{-1} in the first case ($\alpha = \beta = 0$) and V = 0.31 m·y^{-1} in the second one. These values of $V$are quite consistent with the estimate deduced from the water budget at the emergence: in order to supply the Lez spring, (2 m^3·s^{-1} i.e. 63 × 10^6 m^3·y^{-1}), a precipitation area of 63/0.28 = 225 km^2 is required in the first case and 63/0.315 = 200 km^2 in the second one. This is smaller that the catchment area previously quoted (~250 km^2) but not in contradiction with various estimates of the area feeding the spring [Dausse, 2015, Marechal et al., 2014].

4.2. *Detailed interpretation of F_S/K data*

According to (33) the apparent surface heat flow F_S—the residual geothermal heat flow—is equal to the deep heat flow attenuated by a factor e^{-Pe} plus a contribution of the gravity-head potential which tends toward $KG\alpha$ for $Pe \to +\infty$. The last contribution proportional to β and related to the conduit flow is probably very small and therefore neglected; therefore Fs/K should be larger that $G\alpha$ (i.e. 0.23α in °C/100 m). Actually some of the measured thermal gradients are very small and even reach 0. It cannot be excluded that some of these measurements are biased by vertical water circulation inside the well but most measurements seem sound. Since the value of α may be vanishing for these wells, experimental $T(z)$ profiles don't provide any experimental proof for the occurrence of a positive lower bound for the temperature gradient which would indicate some significant positive value of $G\alpha$ for large Pe.

Previous studies have already proposed that gravity potential dissipation does affect the thermal gradient in underground water system [Manga and Kirchner, 2004, Lismonde, 2010]. In particular, Luetscher and Jeannin [2004] compiled observations of vertical temperature gradients in several thick karst systems; these gradients tend toward a small but positive value on the order of 0.3 °C/100 m (i.e. close to G) which could be associated with the dissipation of gravity potential. This result is clearly in contradiction with the present observations of thermal gradients but this also suggests that the temperature gradient was not estimated in the same conditions. According to the present model of saturated porous flow, a lower bound of thermal gradient near to G could occur only for very small fluid pressure (i.e. $\alpha \sim 1$); therefore the occurrence of lower bound close to G would imply that, for such data, water is flowing at pressure conditions which remain close to the atmospheric pressure i.e. in unsaturated conditions at least during part of the flow circuit. Therefore differences in saturation conditions could explain the apparent paradox.

Anyway, the horizontal variations of present observed thermal gradients may be interpreted qualitatively in term of Pe according to $Pe = -\log(F_S/K)$ so

that F_S/K reflects at least qualitatively the local value of the product Vh. According to measurements, a zone of very low gradient values and therefore of large Pe is observed on Figure 6. The wells with labels 3 Mas de Vedel (0.13 °C/100 m), 4 Bois de St Mathieu (0.5 °C/100 m), 6 les Matelles (0.13 °C/100 m), 7 Ferrieres (0 °C/100 m), 25 Frouzet (0.15 °C/100 m), 9 Claret (0.42 °C/100 m) have been drilled in Jurassic layers; all of them are located in recognized zones of water loss physically connected to the Lez spring as shown by dye tracing [Marechal et al., 2014]. This confirms that low thermal gradients areas correspond to high infiltration rate (i.e. high V). Inversely, relatively high values of gradient (> 2 °C/100 m) occur in the eastern and northern border of the catchment; this is consistent with the lack of connection with the spring as observed in these areas by dye tracing [Marechal et al., 2014]. Besides, the polynomial trend of Figure 7 suggests that the central zone of very low thermal gradient (high infiltration?) extends toward the West. This rapid comparison indicates the interest of high precision temperature measurements in shallow boreholes for mapping recharge zones.

4.3. *Global evaluation of integrated energy fluxes*

Due to the small number and values of measured surface gradients, it is impossible to define a single value characterizing the near surface heat flow. Nevertheless an integrated value is available through surface integration of the observed values of F_S over the watershed area would reflect the integrated value of the residual geothermal flux—once part of it is absorbed for heating the water. Evaluation of $E_{\text{resid}} = \int F_S$ requires the knowledge of F_S on the whole area. As the distribution of the available data is uneven and quite sparse, the trend displayed on Figure 7 is used and the surface integral over the whole domain is computed. The resulting residual energy E_{resid} is 5.8 MW. In the interpolation of Figure 7 some negative values of F_S have been obtained in the centre of the basin; when these values are forced to 0, the change in E_{resid} is very small (6.02 MW instead of 5.8). On Table 2 this integral is compared with other values of the energy associated with the system.

The difference between the geothermal flux of deep origin E_{geoth} and that observed at the surface E_{resid} is of the same order as the observed E_{spring} but somewhat smaller by about 25%. It is therefore interesting to study whether the gravity head potential term could contribute significantly to the output temperature: according to the heat budget of the model (33), the component of gravity-head potential should be added as an extra energy to the difference $E_{\text{geoth}} - E_{\text{resid}}$. In the case of $\alpha = 0.1$ which is an upper bound, for $Pe = 6.8$ as suggested in Section 4.1, this component E_{gravity} amounts to 1.08 MW which is significant but clearly too small to explain the gap between E_{spring} and the captured geothermal heat flow $E_{\text{geoth}} - E_{\text{resid}}$. Many explanations for this gap may be suggested: they could proceed from errors in the energy budget such as the underestimate of E_{geoth} or the overestimate of E_{spring}. However this gap could also derive from some inherent simplification of the model; two of them are briefly discussed below.

A first explanation could be that the geothermal heat flow is in fact captured over an area larger than the assumed 250 km^2, as a result of 3D concentration: under this effect, the deep flow lines of the geothermal heat flow would naturally deviate from vertical and tend to converge toward the underground exchanger associated with deep water circulation. As suggested by Badino [2005], this three dimensional effect can be estimated using standard conductive models developed for the design of heat exchangers. Let assimilate the characteristics of the exchanger (the deep conduit) to a horizontal disk with radius $R = 8$ km (area ~ 200 km^2) located at depth $h = 440$ m (simplified geometry required to evaluate its "shape factor" $S_f = 4\pi R/\text{acotg}(R/2h)$) and submitted to a heat flow $K\gamma$ of deep origin. Assume for simplicity that the imposed temperature is 0 at the ground surface and 0 at the disk surface. The linearity of the heat equation allows to superimpose two fields of temperature: (1) the field associated with a disk with imposed temperature $-\gamma h$ and no heat flow at $z = \infty$ plus (2) the field due to a single gradient γz. The absorbed conductive heat flux transferred from the medium to the disk amounts to:

$$E = -KS_f\gamma h + K\pi R^2\gamma \quad \text{with } S_f = 4\pi R/\text{acotg}(R/2h). \tag{40}$$

The result is that the concentration factor increases the absorbed heat flow by only 1%; therefore this natural 3D effect contributes only slightly to the energy gap, except if the deep geothermal flux itself is heterogeneous and exhibits locally a positive anomaly

Table 2. Evaluation of the various integrated energy fluxes

Name	Explanation	Integrated energy (MW)	Corresponding area (km^2)	Average energy flux ($W{\cdot}m^{-2}$)
E_{geoth}	Available geothermal flux over the catchment: $\int K\gamma dS$	21	250	0.085
E_{resid}	Residual thermal flux over the catchment; $\int F_S dS$	6	250	0.021
$E_{geoth} - E_{resid}$	$\int K\gamma dS - \int F_S dS$	15	250	0.064
$E_{gravity}$	Gravity head potential component $PeKG(\alpha h + \beta L/2)$	0 to 1.1	250	
E_{spring}	Output of the spring $(\rho C)\, Q\Delta T$	19	-	-

(not detected by BHT measurements).

A second explanation implies possible transient effects due to external factors forcing such secular variations in water circulation. So far, the budget evaluation use the steady state assumption which rules out such possible environmental changes. The impact of sudden change such as the onset of water circulation can be studied using time dependent solutions of (10)–(15); the time dependent equations are written by replacing "= 0" in (10)–(11) by "$= (\rho C)_r \partial T/\partial t$" and their transient solutions are obtained analytically by Laplace transform followed by numerical inversion. Assume, for example that, starting from an initial conductive equilibrium ($Pe = 0$), the water flow is suddenly switched on with $Pe = 6$ at time $t = 0$. From this epoch up to now, the temperature field evolves toward a new equilibrium and the transient response of the temperature profile propagates downward according to two characteristic times: the diffusive time $\tau_{diff} = z^2/\kappa = 3200$ y (where κ is the rock diffusivity $\sim 2 \times 10^{-6}$ $m^2{\cdot}s^{-1}$) and the convective time $\tau_{conv} = z/V \sim 200$ y (for $V = 0.5$ $m{\cdot}y^{-1}$). Instantaneous temperature profiles are shown in Figure 12a for various values of time following the onset of circulation; they illustrate how the upper layer is quite rapidly cooling whereas the temperature disturbance propagates downward slowly, in the conductive zone $z > h$. The evolution of the conduit temperature as a function of time is also illustrated by Figure 12b, showing that time for reaching the equilibrium temperature is in the order of 10,000 y; this emphasizes the delayed effect of very ancient modifications of the flow which could explain the apparent discrepancy derived from steady state assumptions (e.g. by overestimating the output temperature of the spring and its energy output, since steady state is not yet reached).

5. Conclusion

Available geothermal data around the catchment of the Lez spring offer the opportunity of developing and of applying a geothermal model based on the principle of energy conservation. The energy source is mainly provided by the geothermal heat flux; this energy is exchanged with the fluid during its diffuse flow inside the karstic porous/fractured matrix connected to a conduit until the spring outlet where it is pouring. In order to assess quantitatively the nature and amount of energy captured by this natural heat exchanger, a simplified physical model is developed based on the universal laws of mass and energy conservation in steady state conditions. It leads to second order differential equations for the fluid temperature with boundary conditions which are specific of hydro-geothermal problems encountered in karstic areas. Owing to various simplifying assumptions (simple geometry of the exchanger, negligible horizontal heat conduction) the equations can be solved analytically; simple expressions for temperatures and heat fluxes are proposed as functions of Pe, h plus parameters associated with hydraulic gradients.

This model cannot pretend to account for the actual complexity of the karstic medium but it provides the parameters of a simplified system which is energetically equivalent to the actual flow. The offset observed between the actual ground temperature and the trend of the deep thermal data gives the depth

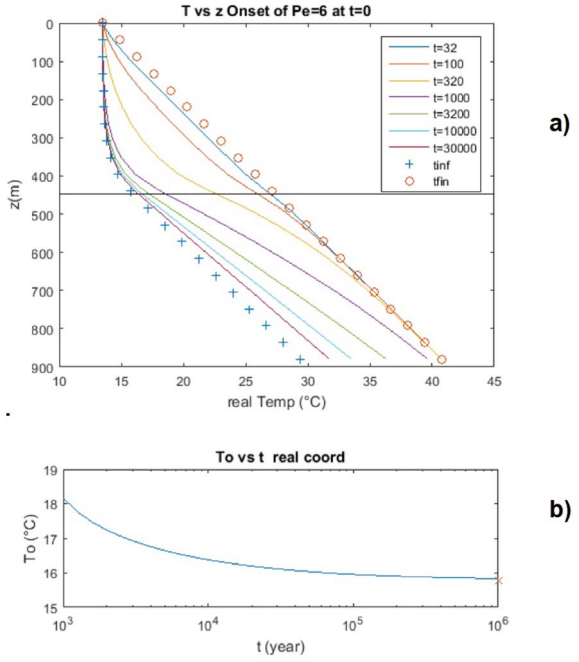

Figure 12. (a) Calculated profiles of $T(z,t)$ resulting from the onset of water circulation ($Pe = 6$) starting at time 0 from a conductive profile. Initial condition (conductive equilibrium) and final one (steady state) are shown as well as several intermediate profiles at various times. The parameters have been adapted to the Lez case ($T_{\text{ground}} = 13.5$ °C, $\gamma = 3.1$ °C/100 m, $h = 440$ m, $Pe = 6$). (b) Resulting temperature T_0 at $z = h$ evolving as a function of actual time in y.

$h \sim 440$ m of the conduit. A mean Peclet number $Pe \sim 6$ can be evaluated from the excess of the spring temperature with respect to that of the rain. An energy budget integrating the various energy fluxes—i.e. (1) deep geothermal flux, (2) residual surface flux deduced from shallow temperature profiles and (3) heat advected at the spring—is presented. The difference between the two first fluxes is insufficient to account for the third one so that a further component of energy is needed. The energy component associated with the dissipation of gravity potential is too small; other explanations are discussed such as 3D effects in the geothermal flux and the occurrence of transient effects due to environmental changes.

In this work, specific attention is directed to the various energy sources affecting fluids, the potential gravitational energy, in particular. Following Stauffer et al. [2014], the correct energy balance transports methalpy, which includes enthalpy (i.e. thermal energy plus fluid pressure) plus the potential energy of gravity, The other terms (kinetic energy and friction energy) are omitted as negligible for porous flow. In water saturated media, the conduction–advection equation for energy involves the transport of hydraulic head H which includes both pressure and gravity potentials; since the vertical fluid pressure gradient tends to compensate the effect of gravity, the contribution of H to the energy balance is much smaller than that of gravity potential alone (which would, on its own, result in a component of vertical thermal gradient up to $G = 0.23$ °C/km) but nevertheless significant. This concept is tentatively applied to the model (and data) of the Lez spring at two levels. Firstly, at the global level, the contribution of gravity-head term is evaluated and could amount to less than 5% of the total energy contribution. Secondly, at the level of single thermal profiles, the gravity and head contribution would eventually result in a lower bound for thermal gradient affected by downward flow; however, from actual thermal profiles obtained in the area, no such lower bound of thermal gradient was evidenced suggesting that the gravity head contribution is not so important.

Data presented here have been obtained in the 80s before recent active management of the Lez output; a systematic campaign of measurements would certainly permit actualization and specify the regional pattern of residual heat flow.

Further investigations and in particular, high precision thermal loggings are required to answer this question definitively, as well as the role of gravitational potential.

Conflicts of interest

The author has no conflict of interest to declare.

Acknowledgments

This work was initiated following discussions with Michel Bakalowicz, Francis Lucazeau, Véronique Leonardi and Hervé Jourde. The development of the mathematical model received assistance from Pierre Genthon. The possible importance of the gravitational potential was pointed out by Patrick

Lachassagne and resulted in discussions with Patrick Goblet, Emmanuel Ledoux and Ghislain de Marsily. The author apologizes for committing a basic error in a previous version of the manuscript while omitting the influence of pressure in the energy budget.

Most of the data come from the collections of CERGA (Centre pour l'Enseignement et la Recherche en Geosciences et Applications) which has been recording and storing most of the hydrogeological studies on the Lez karstic system; the help of Josè Gravellec, Pierre Bérard, Jean Pierre Faillat and Jean Christophe Marechal is gratefully acknowledged.

Appendix A. Analytical solution for a window of the recharge

The singularity of the solution of (23) is associated with the assumption of null horizontal conduction which prevents heat from dissipation at $x = 0$ in the recharge shown on Figure 11a. To avoid this, a convenient approximation consists in modifying the heat budget of the conduit by introducing a further dissipative term; this term simulates horizontal conduction in a strip of porous medium of thickness h' around the conduit. This dissipative term is then—$h'K\partial^2 T/\partial x^2$ and the heat budget is modified according to:

$$h'K\frac{\mathrm{d}^2(T_0 - G\alpha h)}{\mathrm{d}x^2} - (\rho C)_e q\frac{\mathrm{d}(T_0 - G\alpha h)}{\mathrm{d}x} = K\frac{Pe(T_0 - G\alpha h)}{h(1-\mathrm{e}^{-Pe})}T_0 - K(\gamma - G\alpha). \quad \text{(A 1)}$$

With $q = Vx$, this equation becomes:

$$\frac{\mathrm{d}^2(T_0 - G\alpha h)}{\mathrm{d}x^2} - \frac{Pe}{hh'}x\frac{\mathrm{d}(T_0 - G\alpha h)}{\mathrm{d}x} - \frac{Pe(T_0 - G\alpha h)}{hh'(1-\mathrm{e}^{-Pe})} = \frac{1}{h'}(G\alpha - \gamma). \quad \text{(A 2)}$$

The general solution is the sum of the solutions $T_0^* = G\alpha h + (\gamma - G\alpha)h[1-\exp(-Pe)]/Pe$ defined in the main text—cf (28) with $\beta = 0$—plus a combination of two independent solutions of the corresponding homogeneous equation. Using changes $f = (T_0 - G\alpha h)$, $\omega = Pe/(hh')$ and the change of variable $x' = x\sqrt{\omega}$, the homogeneous equation (without second member) becomes:

$$f'' - x'f' - \frac{1}{(1-\exp(-Pe))}f = 0. \quad \text{(A 3)}$$

With the transformation $ff(x') = \exp(x'^2/4)f(x')$, this equation takes the canonical form:

$$ff'' - ff\left[\frac{x'^2}{4} + \frac{1}{(1-\exp(-Pe))} - \frac{1}{2}\right] = 0. \quad \text{(A 4)}$$

Two independent solutions of this equation are the parabolic cylinder functions $u(\mu, x')$ and $v(\mu, x')$ [also called Weber functions by Temme, 2010] which depends on the parameter $\mu = 1/[1-\exp(-Pe)] - 1/2$. Of these two functions, only u has a correct (finite) behaviour for $x' \to \infty$. For large Pe, $\mu \sim 1/2$ and $u(1/2, x') = \sqrt{\pi/2}\exp(x'^2/4)\mathrm{erfc}(x'/\sqrt{2})$. Returning to the (33), the solution which satisfies $T_0(0) = T_{0i} = \gamma h$ and $T_0(x) \to T_0^*$ when $x \to \infty$:

$$T_0(x) = T_0^* + (T_{0i} - T_0^*)\exp\left(\frac{Pe}{2hh'}x^2\right)\mathrm{erfc}\left(\sqrt{\frac{Pe}{2hh'}}x\right). \quad \text{(A 5)}$$

A convenient rational approximation is:

$$T_0(x) = T_0^* + \frac{(T_{0i} - T_0^*)}{1 + 1.5x\sqrt{Pe/2hh'}}. \quad \text{(A 6)}$$

Numeric tests solving the 2D equation with the actual lateral conduction suggest choosing $h' = h/2$ so that $\omega = 2Pe/h^2$. This solution can be extended to the case where $Q = Q_0 + Vx$ i.e. a non zero conduit flow Q_0 at $x = 0$, by replacing x by: $x - Q_0/V$.

References

Atkinson, T. C. (1977). Diffuse flow and conduit flow in limestone terrain in the Mendip Hills, Somerset (Great Britain). *J. Hydrol.*, 35, 93–110.

Avias, J. (1992). Contrôles géologiques des systèmes aquifères karstiques (s.a.k) de type méditerranéen : l'exemple du S.A.K de la source du Lez-France-Karstic aquifers of Mediterranean type, geological controls: Lez Spring (North-Montpellieran karsts, France) example. In *Hydrogeology of Selected Karst Regions*, volume 13, pages 89–113. IAH, Reading.

Avias, J. (1995). Gestion active de l'exsurgence karstique de la source du Lez (Hérault, France) 1957–1994. *Hydrogéologie*, 1, 113–127.

Badino, G. (2005). Underground drainage systems and geothermal flux. *Acta Carstologica*, 34, 277–316.

Bakalowicz, M. (2005). Karst groundwater; a challenge for new resources. *Hydrogeol. J.*, 13, 148–160.

Benderitter, Y., Roy, B., and Tabbagh, A. (1993). Flow characterization through heat transfer evidence in a carbonate fractured medium: first approach. *Water. Resour. Res.*, 29, 3742–3747.

Bérard, P. (1983). Alimentation en eau de la ville de Montpellier. Captage de la source du Lez, commune de St-Clément (Hérault). Etude des relations entre la source et son réservoir aquifère. Rapport no 2.

Birk, S., Liedl, R., and Sauter, M. (2006). Karst spring responses examined by process-based modeling. *Ground Water*, 44, 832–836.

Bonte, D. and Guillou-Frottier, L. (2006). Nouvelles cartographies du flux de chaleur et des températures profondes en France métropolitaine. BRGM report.

Botton, R. (1984). *Etude de certaines modalités du fonctionnement de l'aquifère karstique (zone d'infiltration et zone saturée) sur deux champs de forages Nord Montpelliérains*. PhD thesis, Université Montpellier 2.

Bovardsson, G. (1969). On the temperature of water flowing through fractures. *J. Geophys. Res.*, 74, 1987–1992.

Brigaud, F. and Vasseur, G. (1989). Mineralogy, porosity and fluid control on thermal conductivity of sedimentary rocks. *Geophys. J.*, 98, 525–542.

Burns, E. R., Ingebritsen, S. E., Manga, M., and Williams, C. F. (2016). Evaluating geothermal and hydrogeologic controls on regional groundwater temperature distribution. *Water Resour. Res.*, 52, 1328–1344.

Carslaw, H. S. and Jaeger, J. C. (1959). *Conduction of Heat in Solids*. Clarendon Press, Oxford, 2nd edition.

CERGH (1978). Carte hydrogéologique du Languedoc et du Roussillon. Available from CERGA, Résidence Asterie A2, 740 rue Paul Rimbaud, 34080 Montpellier, France.

Covington, M. D., Luhmann, A. J., Gabrovsek, F., Saar, M. O., and Wicks, C. M. (2011). Mechanisms of heat exchange between water monitoring of ground rock in karst conduits. *Water Resour. Res.*, 47, article no. W10514.

Dausse, A. (2015). *Facteurs d'échelle dans la hiérarchisation des écoulements au sein d'un aquifère karstique - Analyse multi-échelles des propriétés hydrodynamiques et de transport de l'aquifère du Lez*. PhD thesis, Unviversité Montpellier 2.

de Marsily, G. (1995). *Quantitative Hydrogeology*. Academic Press, New York.

Deming, D., Sass, J. H., Lachenbruch, A. H., and Derito, R. F. (1992). Heat flow and subsurface temperature as evidence for basin-scale groundwater flow, North Slope of Alaska. *Geol. Soc. Am. Bull.*, 104, 528–542.

Drogue, C. (1969). *Contribution à l'étude quantitative des systèmes hydrogéologiques karstiques d'après l'exemple de quelques karsts périméditerranéens*. PhD thesis, Université Montpellier 2.

Drogue, C. (1985). Geothermal gradient and ground water circulation in fissured and karstic rocks: the role played by the structure of the permeable network. *J. Geodyn.*, 4, 219–231.

Dubois, P. (1964). Les circulations souterraines dans la région Nord de Montpellier. *Bull. B.R.G.M.*, 2, 1–31.

Ewers, R. and Quinlan, J. F. (1985). Groundwater flow in limestone terranes: strategy national and procedure for reliable efficient monitoring of groundwater quality in karst area. In *National Symposium and Exposition on Aquifer Restoration Ground Water Monitoring, Colombus, Ohio*.

Garibaldi, C. (2010). *Détermination des températures profondes du bassin du Sud-Est de la France et relations entre anomalies thermiques, géologie et circulations hydrothermales par modélisation 3D*. PhD thesis, Université Nice-Sophia Antipolis.

Garibaldi, C., Guillou-Frottier, L., Lardeaux, J. M., Bonte, D., Lopez, S., and Bouchot, V. (2010). Thermal anomalies and geological structures in the Provence basin: implications for hydrothermal circulations at depth. *Bull. Soc. Géol. Fr.*, 181, 363–376.

Ge, S. (1998). Estimation of groundwater velocity in localized fracture zones from well temperature profiles. *J. Volcanol. Geotherm. Res.*, 84, 93–101.

Guilbot, A. (1975). *Modélisation des écoulements d'un aquifère karstique (liaison pluie débit). Application aux bassinsde Saugras et du Lez*. Thése, Université Montpellier 2.

Hassanizadeh, M. and Gray, W. G. (1980). General conservation equations for multi-phase systems. 3 Constitutive theory for porous media flow. *Adv. Water Resour.*, 3, 25–40.

Husson, E. (2013). *Interaction géodynamique/karstification et modélisation géologique 3D des massifs carbonatés. Implication sur la distribution prévisionnelle de la karstification*. PhD

thesis, Université Montpellier 2.

Ingebritsen, S. E., Sherrod, D. R., and Mariner, R. H. (1989). Heat flow and hydrothermal circulation in Cascade range, north-central Oregon. *Science*, 243, 1458–1462.

Karam, Y. (1989). *Essais de modélisation des écoulements dans un aquifère karstique. Exemple de la source du Lez*. PhD thesis, Université Montpellier 2.

Lacas, J. L. (1976). *Introduction à la méthodologie d'étude et d'utilisation des champs hydrothermiques des aquifères karstiques: d'après l'exemple du site de l'exsurgence de la source du Lez (Hérault, France)*. PhD thesis, Université Montpellier 2.

Lachmar, T. E., Freeman, T. G., Sant, C. J., Walker, J. R., Joseph, F., Batir, J. F., Shervais, J. W., Evans, J. P., Nielson, D. L., and Blackwell, D. D. (2017). Effect of an 860-m thick, cold, freshwater aquifer on geothermal potential along the axis of the eastern Snake River Plain, Idaho. *Geotherm. Energy*, 5, article no. 28.

Ladouche, B., Marechal, J. C., and Dorfliger, N. (2014). Semi-distributed lumped model of a karst system under active management. *J. Hydrol.*, 509, 215–230.

Liedl, R. and Sauter, M. (1998). Modelling of aquifer genesis and heat transport in karst systems. *Bull. Hydrogéol.*, 16, 185–200.

Liedl, R., Sauter, M., Huckinghaus, D., Clemens, T., and Teutsch, G. (2003). Simulation of the development of karst aquifer using a coupled continuum pipe flow model. *Water. Resour. Res.*, 39, article no. 1057.

Lismonde, B. (2010). Puissance géothermique advectée par l'eau d'une source et surface de son bassin versant. Étude Théorique. *Karstologia*, 55, 1–10.

Lowell, R. P. (1975). Circulations in fractures, hot springs and convective transport on mid-ocean ridges crests. *Geophys. R. Astron. Soc.*, 40, 351–365.

Lucazeau, F. and Vasseur, G. (1982). Heat flow density data from France and surrounding margins. *Tectonophysics*, 164, 251–258.

Luetscher, M. and Jeannin, P. Y. (2004). Temperature distribution in karst systems: the role of air and water fluxes. *Terra Nova.*, 16, 344–350.

Malard, F. and Chapuis, B. (1995). Temperature logging to describe the movement of sewage-polluted surface water infiltrating into a fractured rock aquifer. *J. Hydrol.*, 173, 191–217.

Manga, M. and Kirchner, J. W. (2004). Interpreting the temperature of water at cold springs and the importance of gravitational potential energy. *Water Resour. Res.*, 40, article no. W05110.

Marechal, J. C., Ladouche, B., Batiot-Guilhe, C., Borrell-Estupina, V., Caballero, Y., Cernesson, F., Dörfliger, N., Fleury, P., Jay-Allemand, M., Jourde, H., Leonardi, V., Malaterre, P. O., Seidel, J. L., and Vion, P. Y. (2014). Projet gestion multi-usages de l'hydrosystème karstique du Lez –synthèse des résultats et recommandations. Rapport BRGM/RP-61051-FR, 126 pp.

Mathey, M. (1974). Gradient géothermique et hydraulique souterraine dans un aquifère karstique (bassin de la source de l'Areuse/NE). *Bull. Soc. Neuchatel. Sci. Nat.*, 97, 301–314.

McLing, T. L., Smith, R. P., Smith, R. W., and Blackwell, D. D. (2016). Wellbore and groundwater temperature distribution eastern Snake River Plain, Idaho: Implications for groundwater flow and geothermal potential. *J. Volcanol. Geotherm. Res.*, 320, 144–155.

Paloc, H. (1979). Alimentation en eau de la ville de Montpellier. Captage de la Source du Lez commune de St Clement (Herault). Etude documentaire prealable a l'etablissement des périmètres de protection. Note de Synthése. Rapport BRGM/79SGN319LRO.

Pimentel, E. T. and Hamza, V. M. (2012). Indications of regional scale groundwater flows in the Amazon Basins: Inferences from results of geothermal studies. *J. South Am. Earth Sci.*, 37, 214–227.

Reiter, M. (2001). Using precision temperature logs to estimate horizontal and vertical groundwater flow components. *Water Resour. Res.*, 37, 663–674.

Saar, M. G. (2011). Review: geothermal heat as a tracer of large scale groundwater flow and a means to determine permeability fields. *Hydrogeol. J.*, 19, 31–52.

Smith, L. and Chapman, D. (1983). On the thermal effects of groundwater flow, I regional systems. *J. Geophys. Res.*, 88, 593–608.

Sposito, G. and Chu, S. Y. (1981). The statistical mechanical theory of groundwater flow. *Water Resour. Res.*, 17, 885–892.

Stauffer, P. H., Lewis, K. C., Stein, J. S., Travis, B. J., Lichner, P., and Zyvoloski, G. (2014). Joule–Thomson effects on the flow of liquid water. *Transp. Porous Media*, 105, 471–485.

Tavares, E., Pimentel, L. C. G., and Hamza, V. M.

(2014). Use of geothermal methods in outlining deep groundwater flow systems in Paleozoic interior basins of Brazil. *Hydrogeol. J.*, 22, 107–128.

Temme, N. M. (2010). Parabolic cylinder function. In Olver, F. W., Lozier, D. W., Boisvert, R. F., and Clark, C. W., editors, *NIST Handbook of Mathematical Functions*. Cambridge University Press, Cambridge.

Thiery, D., Berard, P., and Camus, A. (1983). Captage de la source du Lez: étude des relations entre la source et son réservoir aquifère. Ed. BRGM, 83 SGN 167 LRO, 95 p.

Toth, J. (1963). A theoretical analysis of groundwater in small drainage basins. *J. Geophys. Res.*, 68, 4795–4812.

Touet, F. (1985). *Détermination de l'origine des ressources en eau captées en bordure sud du pli de Montpellier (Hérault)*. PhD thesis, Université Paris XI Orsay.

Uil, H. (1978). *Application du carottage thermique et de l'hydrochimie à l'étude des circulations d'eau souterraine en milieu karstique (région karstique Nord-Montpellieraine)*. PhD thesis, Université Montpellier 2.

Vasseur, G. and Demongodin, L. (1995). Convective and conductive heat transfer in sedimentary basins. *Basin Res.*, 7, 67–79.

Vasseur, G., Demongodin, L., and Bonneville, A. (2002). Thermal modelling of fluid flow effects in thin-dipping aquifers. *Geophys. J. Int.*, 112, 276–289.

Vasseur, G., Lucazeau, F., and Bayer, R. (1985). The problem of heat flow density determination from inaccurate data. *Tectonophysics*, 121, 25–34.

White, W. B. (2002). Karst hydrology: recent developments and open questions. *Eng. Geol.*, 65, 85–105.

White, W. B. (2006). Fifty years of karst hydrology and hydrogeology. In Harmon, R. H. S. and Wicks, C. M., editors, *Perspective in Karst Geomorphology Hydrology and Geochemistry*, Special paper 404. Geological Society of America, Boulder, CO.

Ziagos, J. P. and Blackwell, D. D. (1986). A model for the transient temperature effects of horizontal fluid flow in geothermal systems. *J. Volcanol. Geotherm. Res.*, 27, 371–397.